Final Report of FP7-NMP-2008-EU-India-2, New materials for hydrogen powered mobile applications, Grant Agreement 233482.

Project logo:

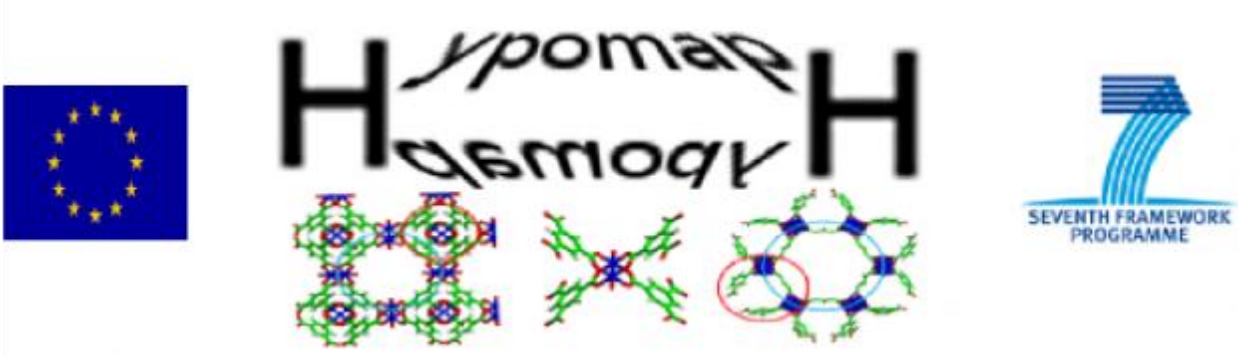

Details of the HYPOMAP project, a joint EU-Indian project in the area of Nanosciences and nanotechnologies, Materials & New Production technologies (NMP),NMP3-SL-2008-233482, including this publishable summary, a list of partners and further information can be found on the project website https://www.jacobs-university.de/ses/theine/projects/HYPOMAP

Please provide an executive summary. The length of this part cannot exceed 1 page.

A challenge today is to responsibly develop and use technologies that will protect our environment. The energy sector is responsible for a large extent of pollution, global warming, and overexploitation of resources. In particular in view of developing nations it is important to develop an alternative energy infrastructure, which avoids fossil fuels, including oil, oil products as gasoline, diesel, kerosene or natural gas. These energy carriers are characterized by low production costs and high energy density. They are hence suitable for mobile applications, but also attractive for stationary electricity production. However, their strongly negative environmental impact creates an apparent danger for our planet and for the well-being of future societies. In particular in the developing countries, but also for the fast implementation and general acceptance in the industrialized nations it is imperative to provide an economically viable alternative to fossil fuels that is sufficient to provide enough energy to the planet, and that can be produced without emission of pollutants, green-house gases and exploitation of natural resources.

A very promising alternative to fossil fuels is the hydrogen economy. Hydrogen, having the highest energy density per mass unit, can be produced by water splitting and its oxidation product is again water, thus creating a cycle without ecological impact. Numerous activities in fundamental and applied research and development concentrate on the production of hydrogen by regenerative energies, in particular by solar energy (photoelectrolysis), the transport of hydrogen in pipelines and tanks, and the direct conversion of the hydrogen's chemical energy into electric energy by highly efficient fuel cells. There are technological solutions available for each individual step that is necessary to form the hydrogen economy, it remains to implement the infrastructure and make those individual solutions – one by one – more efficient and cheaper.

This consortium, composed of Jacobs University Bremen (JacobsUni, Coordinator), University of Calabria (UniCal), CNRS Paris and Montpellier (CNRS) and Stockholm University (SU), concentrated on this latter point: Using computational materials science, it has studied new materials suitable for hydrogen storage and for proton exchange membranes (PEM) in fuel cells. The functioning mechanism of new materials that are available at the lab scale (e.g. metal-organic frameworks (MOF) or polymers functionalized with proton hopping sites for PEM) has been elucidated. Moreover, based on these insights, new materials have been proposed that perform potentially superior to those that are available now. In order to be able to make these analyses and predictions, computational methodology has been developed and is now available to the scientific community.

Further, the consortium has educated 4 PhD students, each of them has become a responsible scientist with awareness to ecological questions. The work has been carried out in close collaboration with an Indian consortium. The relevance of the subject to emerging nations such as India became evident in the research and also in the numerous exchanges that took place. The close cooperation between 4 leading Indian institutions – National Chemical Laboratory Pune (NCL), Bhaba Atomic Research Center Mumbai (BARC), Central Leather Research Institute Chennai (CLRI) and Indian Institute of Technology Kharagpur (IIT) – strengthened and deepened joint Indo-European research and made impact in particular in attracting very talented young Indian scientists to do research in Europe.

Please provide a summary description of the project context and the main objectives. The length of this part cannot exceed 4 pages.

A challenge today is to responsibly develop and use technologies that will protect our environment. This project aimed at developing two important components for the emerging hydrogen economy. Hydrogen can be electrochemically converted directly into electric energy in a fuel cell, a process that avoids combustion engines and that potentially has a very high efficiency. Fuel cell technology is an innovative solution, which addresses local, national, and global environmental needs. Fuel cells running on hydrogen (H_2), derived from a renewable source emit zero carbon dioxide (CO_2) and produce water, which is environmentally benign. Among all known fuels, hydrogen has the highest energy content per unit weight. Switching to a hydrogen economy is in many respects a challenging task. Many issues need to be addressed on the short, medium and long scale. At present, the first hydrogen-powered cars enter small series production (e.g. Mercedes B class), a world-wide standard for hydrogen fueling has been developed and agreed upon, in various countries a network of hydrogen fuel stations has been established, and prototypes of hydrogen powered buses have been introduced at various cities and airports. Still, hydrogen technology is not yet at a sustainable level, and many questions need to be addressed, such as the cheap production of hydrogen (in mid- to long term by renewable energies, in short term from sources such as natural gas), the safe and inexpensive hydrogen storage, and highly efficient conversion of chemical to electric energy through fuel cells need to be resolved. In particular, without effective hydrogen storage systems a hydrogen economy will be difficult to achieve.

This consortium has defined Objectives that aim to improve hydrogen storage solutions and enhance the efficiency of proton exchange membrane fuel cells. The Objectives survey a large range of materials for these purposes, thus allowing a balanced assessment of the different materials classes.

Objectives:

- To study the effect of dopants on H_2 desorption from various destabilized metal hydrides, e.g. MgH_2, complex metal hydrides and metal-organic frameworks (MOFs). In particular the effects of dopant metals on these materials are studied extensively.
- To predict sites of adsorption of H_2 in doped complex metal hydrides and MOFs by quantum chemical calculations and conceptual density functional theory (DFT)
- To accurately calculate the band gaps and subsequently the optical properties of pure and doped ground state and metastable transformations of simple and complex metal hydrides to allow unambiguous characterization of the materials.
- To evaluate the effect of finite temperature on structural and thermodynamic properties of complex metal hydrides and binary hydrogen clathrate hydrates.
- To determine the operation temperature and pressure conditions in which the binary clathrate hydrates desorb hydrogen.
- To study physisorption of molecular hydrogen in porous nanomaterials (carbon-based, MOFs) as function of external temperature and pressure.
- To study simultaneous physisorption/chemisorption in framework nanostructures containing metal clusters
- To study the mobility of guest molecules (H_2 and poisoning N_2 and CO_2) in these frameworks.
- To examine the importance of nuclear quantum effects and isotopic substitution on thermodynamic properties of hydrogen and binary hydrogen clathrate hydrates.
- To investigate different mechanisms proposed for dehydrogenation of amides, alanates and ammonia-borane by organometallic complexes.
- To predict novel and more efficient catalysts for the dehydrogenation process of ammonia-borane on the basis of steric and electronic structure studies.
- To provide a guide to the thermodynamic feasibility of the occurrence of different steps involved in the regeneration of ammonia-borane from the products of dehydrogenation by

determining free energies of reactants, intermediates and products.

- Investigation of new proton-conducting materials for high- and low-temperature fuel cells, based on perovskites and new inorganic nanomaterials like imogolite derivatives (high temperature, HT) and organic substances (low temperature, LT).
- To investigate carbon nanotubes as hydrogen storage material including decorating the nanotubes with metal nanoparticles that can dissociate H_2.
- To investigate hydrogen saturated carbon nanotubes as electrode in fuel cell catalysis.

Please provide a description of the main S & T results/foregrounds. The length of this part cannot exceed 25 pages.

The HYPOMAP project encompassed four Work Packages (WP) where scientific results have been produced. In WP1, scientific methods to address hydrogen storage and proton conductance, have been developed, implemented, and made available to the scientific community, in form of scientific publications and as commercial or free software. In WP2, bulk storage materials have been studied. These encompass classical solid state storage materials such as ammonia boranes and metal hydrates, metastable phases such as clathrate hydrates, and porous nanomaterials such as metal-organic frameworks (MOFs). Thus, hydrogen storage both by chemisorption and physisorption have been addressed. In WP2, we determined the gravimetric and volumetric hydrogen storage capacity of these materials. For clathrates, stability issues have been addressed, and for solid state storage materials where hydrogen is adsorbed by chemisorption the reaction profiles characterizing the loading and unloading of the tanks have been determined. In WP3 we have studied two types of materials, first, fully hydrogenated single-walled carbon nanotubes (SWCNT) that represent probably the best possible gravimetric and volumetric hydrogen storage capacities, but that are not straight-forward to load- and unload. Second, we studied clusters and molecules that may serve as new construction elements for liquid or solid state storage materials. These moieties show exceptional affinity to molecular hydrogen. In WP4, we investigated the atomistic processes taking place in proton exchange membranes (PEM) in fuel cells (FC), and applied this knowledge to design new polymers with enhanced proton conductivity. In the following, we will discuss the main results of the individual work packages.

WP1: Developments

In WP1, led by Prof. Nino Russo of University of Calabria, Italy, the methods, tools, and protocols for the analysis of hydrogen storage and proton conductance calculations have been developed, implemented on various IT infrastructures, and tested. The individual contributions are discussed below in detail, grouped by Deliverables D1.1-D1.5, and by an extra achievement.

All deliverables D1.1-D1.5 of WP1 have been finished and reported before Month 12. D1.1 is the finite-temperature quantized version of density-functional theory for atomic and molecular liquids (QLDFT), which has been developed in two variants of the approximated excess functional, namely the simplest local-interaction expression (LIE-0) and the more sophisticated weighted local-density approximation (LIE-1). D1.2 involves the interaction parameters of molecular hydrogen with various host systems. We have adopted published parameters from the literature to make them technically applicable in our codes, which treat H_2 as a single particle. D1.3 has reached its two main goals: (i) to provide a computer code which allows DFTB calculations of systems containing thousands of atoms, taking advantage of modern algorithms, novel memory models for matrices, and the intrinsic parallel architecture of modern computer processors, and (ii) to provide a comprehensive and validated test of parameters which allows the calculation of various systems which shall be studied in this project in WPs 2-4. Following the same philosophy, van der Waals forces have been introduced using empirical potentials and the class IV/charge model 3 definition of atomic charges (D1.4). D1.5 was concluded by providing a computational package that provides the correct embedding potential for polar surface cluster models, which starts from the unit cell fractional coordinates, generates a finite point charge array enclosed by spherical surfaces, and provides an external potential following this charge

distribution to the core Hamiltonian of the selected quantum method. In addition, we have developed and validated a density functional that reliably provides proton transition state barriers with very high accuracy.

Deliverable D1.1: QLDFT with explicit treatment of intermolecular interactions

A new method to treat fluids in an external potential quantum mechanically, Quantized Liquid Density Functional Theory (QLDFT), has been developed, implemented, tested and published. The approach allows for the calculation of the free interaction energy of hydrogen, as well as other gases or fluids, with any host system. Our model Hamiltonians LIE-0 and LIE-1, parameterized against the experimental equation of state, have been applied to two benchmark systems, bulk fluid hydrogen and hydrogen in a slit pore, and their results compared to those obtained with classical molecular-dynamics simulations employing the same potential and at high temperature, when quantum effects are insignificant. Both functionals produce similar results for direct quantum effects on the adsorption free energy. At the same time, LIE-1 also yields a reasonable description of the fluid structure and classical packing effects, which are not reproduced by LIE-0. The source code of our implementation of the LIE-QLDFT is distributed under the GNU public license and is included as a supporting material of the publication,[1] and available through the project website (Patchkovskii & Heine, 2009).

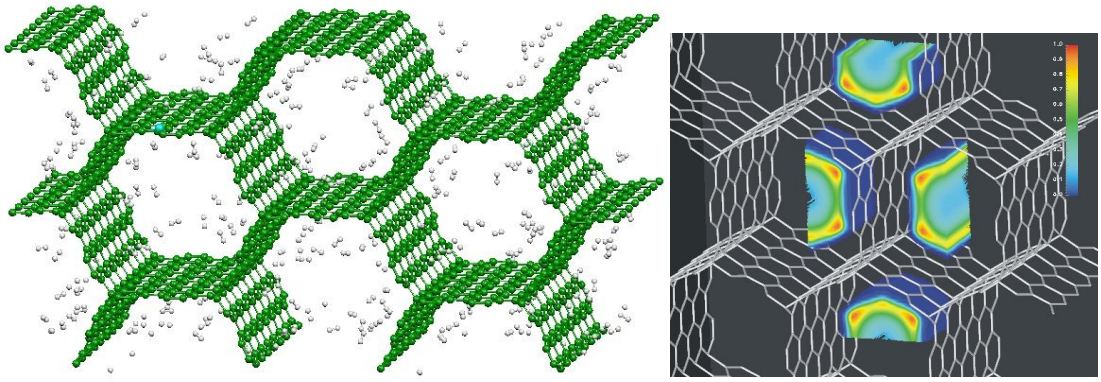

Figure 1. Hydrogen (H_2) distribution in a carbon foam: In classical theory (Grand-Canonical Monte Carlo - GCMC), hydrogen molecules are statistically distributed in the framework (left-hand side). Many configurations need to be considered to describe the thermodynamics of the system properly. In QLDFT (right-hand side), hydrogen is treated as molecular liquid that shows a probability density inside the pore. The thermodynamic properties can be obtained in a single calculation, moreover, quantum effects, considerable for light-weight H_2 in small pores, as well as many-body effects in the hydrogen liquid, are considered in the simulation.

Hydrogen storage capacities of a set of known and modeled porous materials called Porous Aromatic Frameworks (PAFs) give a certain choice of gravimetric and volumetric uptakes. One of them exceeds the 2015 DOE target of gravimetric capacity and the QLDFT simulations go in hand with GCMC simulations of similar materials.[2]

Deliverable D1.2: Database of analytic host-H_2 potentials and parameters which include electrostatic effects, available for QLDFT, MC and MD simulations

Since 2009, a comprehensive set of well-validated interaction parameters between H_2 and host structures, including building blocks of covalent-organic frameworks and metal-organic frameworks, are available in the literature. The consortium has decided to use this data for our own calculations.

Some of our methods, however, require treating H_2 as single, shapeless particles. We have therefore made the parameters from the literature suitable for our methods by spherical averaging using a Monte-Carlo technique. These parameters have been implemented into the QLDFT code and are available to all members of the consortium.

Deliverable D1.3: DFTB code including parameters (C/N/O/B/N/Zn/Cu/H/Nb/Li/Mg)

Density-Functional based Tight-Binding (DFTB) is an approximation to Density Functional Theory (DFT), showing the same qualitative performance at substantially lower computational costs. In order to reach a new quality of system sizes, it was necessary to reimplement this method in order to take advantage of modern developments of computer technology and computational sciences, including the use of sparse matrices and the multi-core architectures of modern CPUs. The new DFTB implementation is available through the deMonNano code. The main features of this software are the possibility to study finite and periodic (infinite) systems on equal footing, the highly efficient computational performance, allowing to study systems in the range 1,000-10,000 atoms, and the interfaces to other built-in methods, in particular molecular mechanics (MM) and DFT, allowing also hybrid high-level – low-level calculations (e.g. QM/MM). The rich functionality list includes features that have been heavily employed in the studies related to Work Packages 2, 3 and 4, namely covering finite and periodic systems; London dispersion corrections, sparse matrix technologies; Car-Parrinello-like molecular dynamics, a robust geometry optimization tool and a frequency analysis driver.

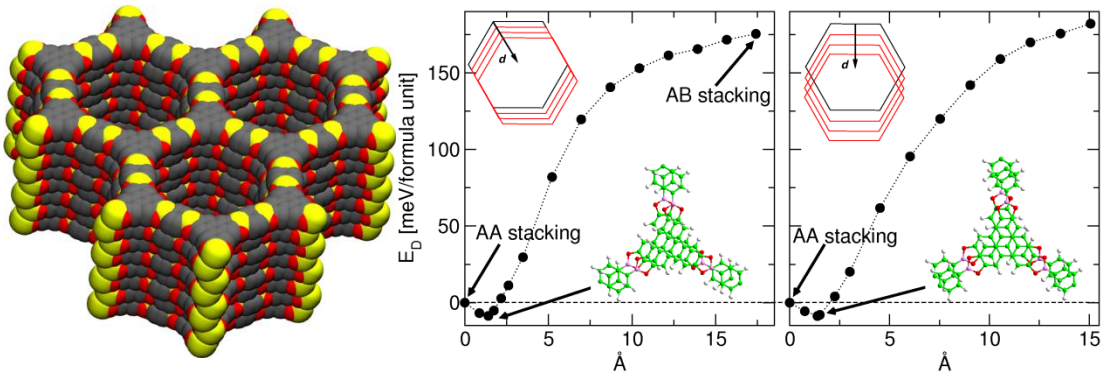

Figure 2. The stacking of Covalent-Organic Framework COF-5: Unlike the AA stacking as originally assumed in experiment, layered (2-dimensional) COFs show a distorted stacking, as indicated in the structure on the left-hand side. This is caused by an interlayer stabilization due to electrostatic and London dispersion interactions (right-hand side).

Deliverable D1.4: DFT code with a posteriori dispersion correction

To complete the panel of systems and interactions treated, a computational protocol, based on Density Functional Theory (DFT) including the London dispersion energy term has also been implemented into the deMon code. The dispersion term is added to the total DFT energy and to the DFT energy gradients (for details see Rapacioli, M et al.[3]). This allows accounting for the weak interactions, although in an empirical way, not only in the computations of the interaction energies, but also in the computations of the structure optimization, of the vibrational frequencies, or when applying the Born-Oppenheimer molecular dynamics technique. The same methodology is

implemented also in the density functional-based tight-binding DFTB method, thus allowing treating systems on a significantly larger scale. The DFTB method is additionally corrected for the calculation of the Coulombic intermolecular potential.

Deliverable D1.5: Embedding procedure for DFT implementations

Systems of interest in this project are typically extended, surfaces, or framework materials. For the exploration of local properties, typically a model system is cut out of the material and treated using methods of quantum chemistry. Most systems studied in this project show a significant redistribution of electronic charge as compared to the free atoms, and hence the electrostatic potential is an important contribution to the Hamiltonian. Therefore, a method has been developed where those contributions can be treated in an efficient way, and implemented to be used in various available computer codes. EMBED is a program package that can be used to model the effects of the surrounding bulk material on a specific area, through a finite point charge array representing the Madelung potential for ionic crystals. Examples and test files, that are included in the distribution package, include tests performed on Al_2O_3, CaF_2, and MgO bulk materials. In addition, we have developed a new exchange-correlation functional which enables us to study proton conductance with the means of relatively inexpensive density functional theory (DFT). The method has been developed, validated and implemented and is available through a commercial product (Gaussian). Details can be found in the publication by the Adamo group.[4]

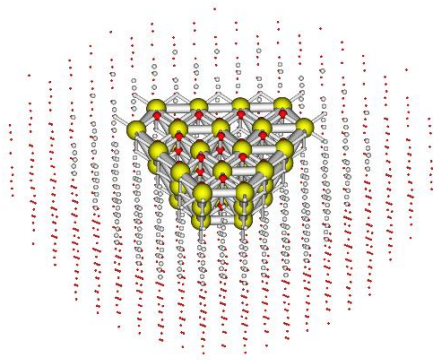

Figure 3. Point charge embedding of a CeO2 cluster.

WP2: Bulk Storage Materials

In a conventional hydrogen storage system, the hydrogen gas is compressed to pressures of 350-700 bar or cooled down to cryogenic temperatures (~ 20 K) and is stored. Both conventional storage possibilities show severe weaknesses: for the high-pressure tanks, a significant amount of energy is needed to compress the gas, advanced materials are needed to form the tank walls, safety issues apply in case of a possible accident (fast gas release, mixture with air and hence danger of explosion), and the volume of the system is still relatively large. For liquid hydrogen tanks, an even larger amount of energy is needed to liquefy the gas and to maintain the very low temperature. Moreover, hydrogen might be released to the environment due to evaporation, leading again to safety issues if the tank is in closed areas.

Storage of hydrogen in a bulk material, either by chemisorption (atomic hydrogen is binding to the bulk system) or physisorption (molecular hydrogen is adsorbed in the system) offer the possibility to store hydrogen gas safely and at higher density, thus making it attractive for mobile applications. Bulk storage systems come with challenges: For **chemisorption**, it first needs to be ensured that the

storage material can be recycled, that is, used and reused for many loading and unloading cycles. As chemical reactions are needed for sorption and desorption, various issues need to be understood and, for potential large-scale applications, tuned. These are

i. The energy balance between loaded and unloaded system should be low, ideally unloading hydrogen should be slightly exothermic.
ii. There must be a significant energy barrier to ensure the stability and hence safety of the hydrogenated system.
iii. Hydrogen release should be controllable, for example by using a catalyst
iv. The system should be reusable, that is, a recycling strategy is in place that can re-hydrogenate the material
v. The gravimetric hydrogen storage capacity should be as high as possible, at least 6 wt%.

In WP2, we have addressed various of the issues mentioned above: In D2.6, we investigate the potential to increase the hydrogen adsorption enthalpy by introducing cations to metal hydrides and metal-organic frameworks. Another possibility of achieving the same goal, studied in D2.7, is to introduce, on purpose, defects into nanostructures that are expected to interact strongly with adsorbed H_2. In view of the application-related goals expressed in D2.6 and D2.7, it is crucial to develop a fundamental understanding of metal atoms interacting with H_2, carried out in D2.8. An interesting solid-state storage system consists of clathrate hydrates, solids with cages defined through intermolecular bonds (i.e. hydrogen bonds). The space in the cages can be used to store hydrogen, and the flexibility in hydrogen bond breaking and formation might be beneficial for loading and unloading those systems. However, clathrates, and in particular their hydrates, show a sensitive thermodynamics that needs to be understood in detail – as depending on pressure and temperature they may release stored gas in an instant and transform from solid to liquid or even gaseous state (see D2.9). Ammonia boranes are well-known bulk storage systems for hydrogen. Due to the low mass of boron and nitrogen atoms, they show very high gravimetric storage capacities, and hydrogen can be released relatively conveniently using thermolysis. Unfortunately, during thermolysis the material reacts into uncontrollable polymeric forms that are difficult to be recycled. Moreover, the exothermic nature of thermolysis makes it difficult to control the hydrogen release reaction. Therefore, we study systems that may develop to become catalysts that control hydrogen release from ammonia boranes in D2.10.

Deliverable D2.6: Novel dopants for various metal hydrides and MOFs to improve hydrogen storage

The hydrogen storage properties of MOF-5 have been improved by metal ion decoration of the organic linkers. In this respect, doping by Li^+, Na^+, Mg^{2+} and Be^{2+} were studied and it was found that Mg^{2+} increases the hydrogen absorption energy of MOF-5 to the desired reversible hydrogen storage level. To improve the hydrogen absorption of MOF-5, the metal atom decoration was also studied and it was found that lithium and aluminum desorption increases the hydrogen adsorption significantly. BH_3 doped B- substituted MOF-5 was also studied and it was found that BH_3, being an electron deficient molecule helps the hydrogen adsorption in the presence of B atom. The scandium doped MOF-5 was also studied and it was seen that the adsorption energies improve as a result of doping by this light transition metal.[5]

The hydrogen storage capacity of Li^+, Na^+ and K^+ doped Boric acid clusters have been investigated.[6] The storage capacity and gravimetric density of the bowl-shaped cluster (BA5) was found to be higher than for the sheet (BA6) and ball (BA20) structures.

The nature of the interaction between molecular hydrogen and various fragments of metal organic framework materials has been studied. Based on this a new MOF material has been designed and its hydrogen storage capacity has been compared with the native MOF. With a view to improve the hydrogen storage capacity of MOF, various strategies, like ligand replacement and chemical functionalization of the organic linker, have been adopted. It has been found that inclusion of open metal sites increases the hydrogen storage capacity of the MOF. Substantial improvement in the adsorption enthalpies suggests reasonable hydrogen storage at ambient conditions.[7]

We explored the possibility of improving the light metal binding energy, as well as the hydrogen adsorption energy, in MOF-5 through boron doping. The metal atom interaction energies with MOF-5 are found to be very strong, and are high also compared with the metal cohesive energies. In the case of lithium and sodium -decorated MOF- 5, the gravimetric hydrogen densities are found to be 4.3 and 7.4 wt % respectively.[8]

A systematic study of the electronic structure and properties of the aluminum hydrides which are analogues to the boranes has been carried out. Under this, we have studied different classes of hydrides, viz., closo (Al_nH_{n+2}), nido (Al_nH_{n+4}), and arachno (Al_nH_{n+6}).[9]

Deliverable D2.7: Fundamental effect of defects on nanostructures

We modeled a novel porous doped fullerene $C_{24}N_{24}$ generated through the truncation doping of 24 carbons of C_{60} with 24 nitrogens. This fullerene is found to bind transition metals more effectively to avoid the metal clustering. These metal-doped fullerenes are found to adsorb molecular hydrogen at a gravimetric capacity of ~5.0 wt%.[10]

Deliverable D2.8: Fundamental understanding of H_2 interaction with metal atoms

Metal hydrido-amine complexes (metal = Ru, Rh, and Ir) attract ever increasing attention as highly active and enantioselective transfer hydrogenation catalysts. The key feature of most transfer hydrogenation catalysts is the presence of a hydridic M-H subunit adjacent to a protic N-H functionality. In neutral and basic conditions the catalyst transfers these two hydrogen atoms to polar unsaturated substrates, avoiding direct coordination of the substrate to the metal. As a consequence of this hydrogen transfer, the catalyst is converted into a 16-electron amido entity through a six-membered ring transition state. Then, in the catalyst regeneration step, dihydrogen sources provide H_2 to the amido complex to re-form the 18-electron amino-hydride. We investigate[11] by DFT the mechanistic details of the overall reaction of the iridium transfer hydrogenation catalyst Cp*Ir(TsDPEN-H) with H_2 and O_2 with the support of experimental observations and the proposed reaction mechanism. We believe this work could contribute to enhance further understanding and provide helpful information that would inspire the design of new catalysts for fuel cells.

In addition we explored the interaction of a series of uranium oxide anions with small organic substrates in order to investigate if these catalysts can be proposed for H_2 production. The following computational protocols were employed: the Zero-Order Regular Approximation (ZORA) was used in combination with the PW91 functionals (exchange and correlation) and the TZ2P (TZP for uranium)

basis set or the hybrid B3LYP functional was employed together with the Stuttgart-Dresden RECP basis sets for the metal center. Results[12] show that the gas phase reaction favors the elimination of the hydrogen molecule both from a thermodynamic and kinetic point of view.

The mechanistic details of the reaction that occurs in the fuel cell between oxygen and hydrogen in the presence of catalysts were studied by using first principles methods. In particular, the hydrogenation of molecular oxygen by the 18e amino-hydride

Cp*IrH(TsDPEN) (1H(H)) complex to give Cp*Ir(TsDPEN-H) (1) and 1 equiv of H_2O were investigated by means of hybrid density functional calculations (B3LYP). To describe the overall catalytic cycle of the hydrogenation of dioxygen using H_2 catalyzed by the Ir complex 1, the potential energy surfaces for the hydrogenation process of both the catalyst 1 and the corresponding unsaturated iridium(III) amine cation ($[1H]^+$) were explored at the same level of theory. The results of our computations, in agreement with experimental findings, confirm that the addition of H_2 to the 16e diamido complexes 1 is favorable but is slow and is accelerated by the presence of Brønsted acids, such as HOTf, which convert 1 into the corresponding amine cation [1H]+. By deprotonation of the subsequently hydrogenated $[1H(H_2)]^+$ complex the amine hydride catalyst 1H(H) is generated, which is able to reduce molecular oxygen. Preliminary results concerning the O_2 reduction in acidic conditions show that the reaction proceeds by intermediate production of H_2O_2, which reacts with 1H(H) to eliminate water, restore $[1H]^+$, and restart the catalytic cycle. The energetics of the process appears to be definitely more favorable with respect to the analogous pathways under neutral conditions.

Furthermore, the possible release of H_2 from reactions of HUO_3 ions with CH_3OH substrates has been considered. The reaction is thermodynamically exothermic and the energetic barriers necessary to produce H_2 lie below the reactant energies.

The hydrogen trapping ability of various metal clusters, boron lithium cluster, lithium-doped borazine derivative, lithium doped boron hydride and metal-doped N_4 and N_6 rings are studied at various levels of theory. Different types of interaction energies, reaction enthalpies and conceptual DFT based reactivity descriptors provide important insights into the associated interactions. The negative ΔG region is dictated by the T-P phase diagram. The noble gas trapping ability of H^{3+} and Li^{3+} is also analyzed. The hydrogen trapping ability of various metal – ethylene complexes is assessed computationally. There exist two distinct classes of bonding patterns, viz., a Kubas-type interaction between the metal and the H_2 molecule behaving as an η^2-ligand and an electrostatic interaction between the metal and the atomic hydrogen.

Hydrogen storage capacities of some $Li+/F^-$ doped neutral and charged aromatic/antiaromatic systems are studied at various levels of theory. Various CDFT based global and local reactivity descriptors, nucleus independent chemical shift (NICS), NICS-rate, interaction energy per H_2 molecule, reaction enthalpy and reaction electrophilicity are used for this purpose.

The hydrogen storage ability of some lithium decorated star-like clusters and super-alkali systems is assessed at the M06/6-311+G(d,p) and M052X/6-311+G(d) levels, respectively. The effect of an applied electric field on the hydrogen binding energy is also analyzed.[13]

Ionization potential and electron affinity of several neutral atoms and their cations, dications, anions, and dianions in gas and solution phases have been calculated at various levels of theory.[14]

Potential use of some alkaline-earth metal cages, alkali-metal clusters[15] and Li-doped boron hydrides,[16] metal-aromatic systems[17] and metal-ethylene compounds[18] for the storage of hydrogen was analyzed using conceptual DFT.[19]

Aromaticity[20] and hydrogen storage capability of N_6^{4-}, N_4^{2-} rings[21] were also explored. The ab initio and DFT studies on hydrogen storage on some Li^+/F^- doped aromatic/antiaromatic systems reveal that there is a direct connection between the hydrogen adsorption potential and the aromaticity/antiaromaticity of the same as well as the charge on it or on a reactive center therein. While the aromaticity takes care of the stability, the charges help in hydrogen adsorption through electrostatic interactions.[22]

Hydrogen adsorption properties of different carbon annulene systems, C_nH_n (n=4, 5 and 8) decorated with alkali metal atoms were studied.[23] C_5H_5-Li is found to have better hydrogen adsorption properties with a gravimetric capacity of 12.0 wt%.

Hydrogen adsorption properties of star-like silicon-lithium binary clusters were carried out.[24] Si_5Li^{7+} is found to adsorb 15 molecules of hydrogen with interaction energy of ~2.5 kcal/mol and the corresponding hydrogen gravimetric density is 13.7 wt**%.**

We have studied the structure, stability and hydrogen adsorption properties of different boron hydrides decorated with lithium, examples of the corresponding anions being dihydrodiborate dianion, $B_2H_{22}^-$ and tetrahydrodiborate dianion, $B_2H_{42}^-$ which can be considered to be analogues and isoelectronic to acetylene (C_2H_2) and ethylene (C_2H_4), respectively.[25]

Ab initio studies on molecular hydrogen adsorption in lithium-doped hexaborane(6) ($B_6H_6Li_2$) have been carried out.[26] Each lithium site is found to adsorb a maximum of three hydrogen molecules which corresponds to a gravimetric density of 12 wt %. We have also verified the possibility of constructing a three-dimensional solid using the dilithium-doped B6 unit as a building block and -C≡C- units as linking agent which can adsorb hydrogen with a gravimetric density of 7.3 wt %.

We have investigated lithium-dispersed two-dimensional carbon allotropes, viz. graphyne and graphdiyne, for their applications as lithium storage and hydrogen storage materials.[27] Our calculated hydrogen adsorption enthalpies (−3.5 to −2.8 kcal/mol) are very close to the optimum adsorption enthalpy proposed for ambient temperature hydrogen storage (−3.6 kcal/mol)

The molecular hydrogen adsorption in binary all-metal aromatic systems, viz. Be_3M_2, Mg_3M_2 and Al_4M_2 (M = Li, Na and K) has been explored using ab initio quantum chemical calculations.[17] Al_4M_2 are found to be more suitable and the gravimetric densities of hydrogen in hydrogenated Al_4Li_2 and Al_4Na_2 are calculated to be respectively 11.59 and 9.4 wt% .

Deliverable D2.9: Thermodynamic properties of clathrate hydrates

Structure, stability, and reactivity of clathrate hydrates with or without hydrogen encapsulation are studied using standard density functional calculations. Conceptual density functional theory-based reactivity descriptors and the associated electronic structure principles are used to explain the hydrogen storage properties of clathrate hydrates. Different thermodynamic quantities associated with H_2-trapping are also computed. The stability of the H_2-clathrate hydrate complexes increases upon the subsequent addition of hydrogen molecules to the clathrate hydrates. The efficacy of trapping hydrogen molecules inside the cages of clathrate hydrates in an endohedral fashion depends on the cavity sizes and shapes of the clathrate hydrates. Computational studies reveal that

structures 512 and 51262 are able to accommodate up to two H_2 molecules whereas 51268 can accommodate up to six hydrogen molecules. Adsorption and desorption rates conform to that of a good hydrogen storage material.

Molecular Dynamics Study on SI Clathrate Hydrate. A Classical molecular dynamics study is performed on type S-I clathrate containing 9936 water molecules in a 6x6x6 unit cell.[28] The extended simple point charge (SPC/E) water model is used and periodic boundary conditions are employed.

The type S-I clathrate is found to be stable at low temperature and high pressure. Now we are trying to generate the T-P phase diagram of the hydrogen-loaded S-I clathrate with and without guest molecule. We are using the LAMMPS package for this simulation purpose.

Deliverable D2.10: New catalysts for dehydrogenation of boron nitrides

Ammonia borane (AB) dehydrogenation is a very important topic, because of the potential of AB for chemically storing hydrogen. Many catalysts have recently been reported that can catalyze AB dehydrogenation, but almost all of them are transition-metal-based systems. If AB were indeed to become the primary means for storing hydrogen in the near future, organocatalysts will have to be employed for its dehydrogenation because such systems enjoy the advantages of (i) being cheap and (ii) environmentally friendly. To date, no organocatalyst has been designed that can efficiently dehydrogenate AB. What we have attempted is a study of whether recently synthesized organic cage structures have the potential for catalyzing AB dehydrogenation. Full quantum mechanical calculations have been carried out for testing such systems. The barriers found for the dehydrogenation process for the caged organocatalysts indicate that such caged structures indeed could function as catalysts for dehydrogenating AB. Moreover, modifications to the cage structures have been proposed and studied, with the results indicating the potential of the newly proposed structures to be excellent multi-site catalysts for dehydrogenating AB through different competitive pathways.[29]

Computational DFT and MP2 studies have been performed to investigate the interaction between the iridium dihydrogen pincer complex: (POCOP)IrH_2 (where POCOP =$\eta^3$1,3(OPtBu_2)2C_6H_3) and NH_2BH_2, the immediate product of ammonia borane (NH_3BH_3) dehydrogenation. A mechanism has been proposed for an oligomerization process at the metal center that involves competition between (i) insertion of an NH_2BH_2 molecule into the $(NH_2BH_2)_n$ chain and (ii) termination of the chain leading to the formation of the cyclic $(NH_2BH_2)_n$ oligomer. The calculated ΔG values show that the competition favors insertion over termination for the cases n=1 to n=4 but favors termination for n=5. The computational studies therefore indicate that the cyclic pentamer $(NH_2BH_2)_5$ would be formed during NH_3BH_3 dehydrogenation by the (POCOP)IrH_2 catalyst, agreeing with experimental findings. The mechanistic understanding gained has implications for the facile regeneration of ammonia borane.[30]

The recently synthesized rhodium complex [Rh{$P(C_5H_9)_2(\eta^2\text{-}C_5H_7)$} $(Me_2HNBH_3)_2$][BarF], which incorporates two amine-boranes coordinated to the rhodium center with two different binding modes, namely η^1 and η^2, has been used to probe whether bis (amine-borane) motifs are important in determining the general course of amine-borane dehydrocoupling reactions. DFT calculations have been carried out to explore mechanistic alternatives that ultimately lead to the formation of the amine-borane cyclic dimer $[BH_2NMe_2]_2$ (A) by hydrogen elimination. Sequential concerted, on- or off

metal, intramolecular dehydrogenations provide two coordinated amineborane molecules. Subsequent dimerization is likely to occur off the metal in solution. In spite of the computationally confirmed presence of a BH•••NH hydrogen bond between amine-borane ligands, neither a simple intermolecular route for dehydrocoupling of complex 2 is operating, nor seems $[Rh\{P(C_5H_9)_2\text{-}(\eta^2\text{-}C_5H_7)\}B]^+$ to be important for the whole dehydrocoupling process.[31]

New main-group catalysts have been proposed and investigated for the dehydrogenation of ammonia borane.[29, 32]

WP3: Nanoporous materials

In WP3, the features of adsorption, spillover and diffusion are given the main attention. Spillover is a way to store dissociated molecular hydrogen and store it by chemisorption. It involves dissociation of hydrogen gas by supported metal catalysts, subsequent migration of atomic hydrogen through the support material and final adsorption in a sorbent. As the final sorption is chemisorption, the surface area of the sorbent is more important than the pore volume. D3.11-D3.15 address issues related to spillover on single-wall carbon nanotubes (SWCNT) with supported platinum clusters. D3.11 shows the development of two sets of DFTB parameters of Pt with C and H along with their successes and limitations. Due to some delays and the limitations, studies of hydrogen atom diffusion, spillover mechanism (D3.13) and their recombination (D3.14) were studied using DFT rather than the envisaged DFTB. With some experimental insight, the initial idea of cartridges loaded with hydrogenated nanotubes working as anode in the fuel cell (D3.15) is now realized as not feasible.

Calculations of gravimetric and volumetric storage capacities of nanostructured materials are given in D3.16. Quantum effects are found to be significant in adsorption calculations (D3.17). Interesting results on chemi- and physisorption in nanostructured materials are detailed in D3.18. A database of diffusion constants of various gases in nanoporous materials for the deliverable D3.19 is currently compiled by the Indian partners and will be made available on the project website.

Deliverable D3.11: DFTB parameters for interaction of selected metal particles with SWCNT

The objective is to develop parameters for a simplified description of H_2 gas dissociating over nano-particles, initially of Platinum, supported on single-wall carbon nanotubes (SWCNT) and the spillover of hydrogen onto the nanotube and subsequent diffusion. Therefore, an efficient computational protocol, incorporating the DFTB method (see D3) for the calculation of the interaction of hydrogen with metal-decorated SWCNTs, has been developed. DFTB interaction parameters for Pt-Pt, C-Pt, and H-Pt have been generated and validated by comparing benchmark systems for which high-quality theoretical and experimental data were available.

The objective is to develop parameters for a simplified description of H_2 gas dissociating over nano-particles, initially of Platinum, supported on single-wall carbon nanotubes (SWCNT) and the spillover of hydrogen onto the nanotube and subsequent diffusion. As calibration and reference we have determined structure and interaction with hydrogen for a sequence of small gas phase Pt_n clusters (n=2-9, 13 and 38) using the newly developed real-space-grid-based GPAW full DFT code as well as studied Pt_4 on two model SWCNT's. In addition, we have computed the band structure of bulk fcc Pt as well as that of a linear chain of Pt atoms. For the simplified description we explored tight-binding in both DFTB and the newly developed HotBit code, as well as investigated ReaxFF (an empirical

force-field that allows dissociation) as an alternative description. ReaxFF was, however, deemed unsuitable for the purpose of the present project and was abandoned. Since initially we did not have full access to all programs necessary for the development of tight-binding (TB) parameters within DFTB we shifted focus to the HotBit code, which is a development parallel with GPAW. Both HotBit and GPAW use the very convenient Python-based Atomic Simulation Environment (ASE) package but since both codes are under development we have spent some effort to develop and implement features which were necessary for the treatment of heavy metals in HotBit in collaboration with the HotBit team in Jyväskylä, Finland, and for the treatment of inner-shell spectroscopies in GPAW (x-ray photoemission spectroscopy (XPS), X-ray absorption spectroscopy (XAS) and X-ray emission spectroscopy (XES)[33] to relate to the experimental techniques in the characterization of the hydrogenated nanotubes. The idea is to use the tight-binding approximation to investigate large and realistic models of nanotubes interacting with nanoparticles and hydrogen including temperature-dependent dynamics. Interesting situations will subsequently be studied using smaller models that allow higher-level computational approaches to relate directly to the experimental probes.

Parameters for a tight-binding description have been optimized and validated for Pt-Pt, Pt-C, and Pt-H interactions. The parameter sets are available on the project website. A manuscript is planned describing the results.

We have tested our C and H parameters for DFTB calculations and they perform very well for a large set of carbon-based materials.[34] On the other hand, the tight-binding parameters of Pt are much more complicated and we have learned that the standard protocol of parameterization is not sufficient to obtain transferable tables. Relativistic effects and spin-orbit corrections are very important, which were missing in the standard protocol. While simple Pt clusters can be successfully optimized with the previously created tables, addition of carbon-based materials failed badly. Therefore, we would not claim transferability of our present parameters.

We have studied the parameterization of Pt in detail and the results are not very conclusive. While, for some test models they perform quite well, for others they failed badly. We have concluded that Pt parameters require special treatment and one of the most important key-factors are relativistic effects and the spin-orbit correction. The main deviation from the DoW is that ultimately we have instead performed more costly calculations using the full DFT level of theory in order to fulfil the deliverables D3.13 and D3.14, and to understand the spillover mechanism in hydrogen storage on metal-decorated SWCNTs.

We have created a set of parameters for Pt/C/H elements. While parameters for the light elements perform excellently and successfully pass sever validation calculations, the parameters for Pt do not give conclusive results. To compensate for the DFTB results and to understand the spillover mechanism of H_2 onto SWCNTs we have performed several cluster model calculations at the full DFT level of theory (see D3.13 and D3.14).

Deliverable D3.12: Progress report on H_2 dissociation

Two aspects of H_2 dissociation are discussed here in this progress report. The first, as mentioned in the proposal, discusses the dissociation of H_2 on platinum clusters, investigated by means of high-level DFT calculations. We have studied sequential hydrogen dissociative chemisorption on a series of Pt_n clusters (where n=2-9, 13 and 38) to address and understand their catalytic activity towards H_2 dissociation. In case of each cluster, the preferable adsorption site (one-fold on-top, two-fold bridge and three-fold hollow) has been explored. We find the on-top site to be the energetically most

favorable binding site, followed by the edge site. The barriers for the H_2 dissociation have also been determined. The second aspect of H_2 dissociation that is discussed deals with the dissociation of H_2 from catalytic reaction systems where H_2 is dissociated from ammonia–borane (AB). Experimentally, the iridium pincer complex, [(POCOPtBu)Ir$(H)_2$], has been found to be the most effective catalyst for hydrogen dehydrogenation and dissociation from AB. However, its limitation lies in the fact that it is able to dissociate only one equivalent of H_2 while other catalysts have been demonstrated to produce two or more equivalents of hydrogen. This limited dissociation of H_2 in the case of AB reduces its efficiency. Experimental studies with different AB dehydrogenation catalyst systems have shown that all systems that produce the polyborazylene (PB) oligomer produce two or more equivalents of H_2 while the iridium pincer ligand catalyst system is seen to be unique in producing the cyclic pentamer, $(NH_2BH_2)_5$. It is clear that an understanding of the reasons for the formation of the cyclic pentamer rather than PB will help understand why further dissociation of H_2 does not occur for the iridium pincer ligand system. The objective of the current study has been to do just that so as to unlock the full potential of the iridium pincer ligand catalyst system. The full mechanism for the cyclic pentamer formation process has thus been determined in this work package, using DFT calculations.

(i) The barrier to dissociation of H_2 on platinum clusters

Over the range of clusters we find that the H_2 dissociative chemisorption energy fluctuates in the range between 0.89-1.09 eV, which is around 0.2-0.3 eV higher than the experimental value for the H_2 dissociative chemisorption on the Pt(111) surface at zero coverage. We also observed that the sequential hydrogen desorption energy varies in the range 2.44-2.58 eV, i.e. slightly smaller than the value reported earlier for an isolated H atom on the Pt(111) surface. As a result of this study, we can conclude that the H_2 dissociative chemisorption energy on these clusters does not change significantly with cluster size and shape.

(ii) The pathways and barriers to H_2 dissociation

We further studied the reaction pathways of hydrogen dissociation on Pt_{13} and Pt_{38} clusters. Dissociation of H_2 over the on-top site is found to proceed without a barrier and subsequent diffusion barriers are lower than 0.33 eV. The final product has a chemisorption energy of 1.64 eV with two hydrogen atoms well separated at bridge sites. As a result of these calculations, it is very clear that H_2 dissociation is possible on the top sites, which supports the catalytic activity of the clusters of this size. Moreover, these calculations are consistent with earlier reported results where dissociation of molecular H_2 on Pt surfaces/clusters has been shown to proceed with low or no barrier, in addition to high mobility of dissociated H atoms. This calculation also suggests that H atoms can readily overcome the moderate activation barriers and migrate from top sites to the more favorable bridge sites. Similar results are found for the Pt_{38} cluster except for a slight decrease in adsorption energy with growing cluster size

(iii) Determination of the role of the iridium pincer ligand complex in the formation of the cyclic pentamer $(NH_2BH_2)_5$.

The DFT investigations that we have conducted in this study demonstrate that the iridium catalyst complex is instrumental in producing the experimentally observed exclusive formation of the cyclic pentamer, $(NH_2BH_2)_5$, because it traps the amino borane complex, NH_2BH_2, which then subsequently undergoes the addition of more amino borane units at the metal center. This corroborates the

experimental findings using ^{12}B NMR published in the literature that show that the iridium pincer complex is unique in not allowing the amino borane product, NH_2BH_2 to move into the solution after formation, where, in the case of all the other catalysts, it is able to catalyze the further dissociation of H_2 and eventually form the product PB. The complete mechanism for the production of the cyclic pentamer has been determined and the reason for the exclusive formation of the pentamer has been understood. The results of the study indicate that there are two competing processes during the oligomerization: the insertion of the monomer, NH_2BH_2 to the oligomer chain bound at the iridium center, and the termination of the said chain to yield the cyclic oligomer. The interesting finding from the calculations is that the termination to the cyclic oligomer becomes more favorable than the insertion of monomer only when the oligomer length has increased to five NH_2BH_2 units. This is the reason why the cyclic oligomer is formed in quantitative yield during the reaction.

(iv) Possible role of the solvent, THF, as well as of the observed dormant species of iridium in the formation of the cyclic oligomer, $(NH_2BH_2)_5$.

The calculations also indicate that the solvent used during the catalysis (THF), as well as the dormant species observed during the catalysis, $[(POCOPtBu)Ir(H)_2(BH)_3]$, can also play a role in the oligomerization process. We have demonstrated that the amino borane species can insert into the Ir-B bond, and thereby lengthen the chain, with the solvent, THF, serving to sever the BH_3 from the complex prior to the termination step.

With regard to the dissociation of H_2 on platinum clusters, there is no deviation in the work conducted with respect to what was proposed. With regard to the work reported here on H_2 dissociation from ammonia borane, AB, it is noted here that this work done is in addition to what had been proposed for H_2 dissociation in the proposal, where the focus was primarily on H_2 dissociation from platinum clusters. The work done with AB will also help in the development of new catalysts for H_2 dissociation from AB, thereby satisfying other deliverables of the project.

In conclusion, we have studied the dissociation of H_2 on platinum complexes through DFT calculations and found the process to be quite favorable for different cases of platinum clusters. In addition, we have endeavored to understand, in full, the mechanism for the formation of the cyclic $(NH_2BH_2)_5$ pentamer. This has been deemed necessary so as to determine the means of increasing the dissociation of H_2 from AB-iridium pincer catalyst complexes. The mechanism has been thoroughly understood through DFT calculations

Deliverable D3.13: Progress report on H atom diffusion and spill-over onto SWCNT

The objective of this part of the work was to investigate the adsorption, dissociation and subsequent diffusion of H_2 or H on carbon nanotubes. There are two parts to the work: first, the adsorption of a tetrahedral Pt_4 cluster on a (10,0) SWCNT is discussed as a model to gain insight into the catalytic and adsorption behavior of Pt supported on SWCNT. Discussed next is the work done to investigate the hydrogen adsorption and diffusion on SWCNT. The work done indicates that the diffusion of hydrogen on SWCNT is a highly unlikely process but instead that the Pt cluster could be more mobile.[34]

(i) Adsorption of Pt_4 clusters on (10,0) and (5,5) SWCNTs

Pt_4 being a small cluster on the SWCNT support exhibits structural flexibility. Out of many possibilities we selected three representative structures of Pt_4 on a (10,0) SWCNT: 1) one Pt atom in direct contact with the nanotube, 2) two Pt atoms in contact with the nanotube and 3) three Pt atoms in contact with the nanotube. We observed that the adsorption energy (1.54, 1.99 and 2.32 eV) increases with increasing number of Pt-C contacts. This also means that Pt-C bonds play a major role in the structural stability of Pt clusters on the SWCNT support. In order to investigate the mobility of the Pt_4 clusters on the SWCNT support proceeding through structural conversions, we calculated the energy barriers for interconversion pathways between the three most likely structures of the chemisorbed Pt_4 cluster. We found that the energy barriers between these three structures vary from 0.09 to 1.18 eV. Similar calculations have been performed for the (5,5) SWCNT to check the effect of curvature on the barrier heights.

(ii) Hydrogen adsorption and diffusion on SWCNT

In order to understand the most plausible reaction path for the dissociation of hydrogen on SWCNT, we explored several initial hydrogen adsorption configurations. The binding energy was seen to vary from -0.04 to 0.27 eV in the different configurations studied. In addition to this, the hydrogen dissociative adsorption reaction profile was calculated for the different configurations. Furthermore, the possible pathways of hydrogen diffusion in the configurations were studied and the possible mechanisms for the diffusion examined. All pathways studied were found to be associated with high barriers to diffusion with the lowest barrier for diffusion found to be 2.22 eV. This suggests that the diffusion of hydrogen over SWCNT is a highly unlikely process.

(iii) Results for hydrogen adsorption and barrier for dissociation on small Pt_4 clusters

Using DFT, we have studied hydrogen chemisorption on a small Pt_4 cluster to address and understand its catalytic activity towards H_2 dissociation. We have found that the H_2 molecule in the presence of a Pt cluster dissociates without barrier and the total energy of the system will be lowered significantly (see Figure 4).

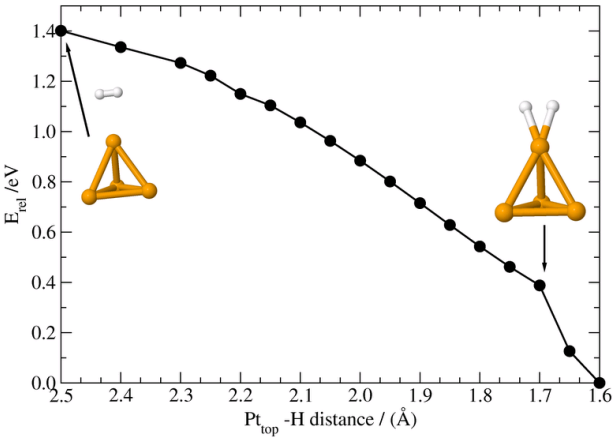

Figure 4. Relative energy plot versus the distance of the H_2 molecule from the Pt_4 cluster.

We have also investigated if the Pt cluster can split the H_2 molecule and bind it directly to the carbon surface when the two species are on opposite sides of the carbon surface; this models the case when

the metal particle is inside the SWCNT. The results show that the energy barrier for such a reaction is very high and most certainly unlikely (~8 eV activation energy).

(iv) Adsorption of Pt_4 clusters and H_2 molecules on a carbon flake with curvature of the (10,10) SWCNT

We have chosen finite model structures for our calculations. To represent the influence of a carbon nanotube, our model was a carbon flake $C_{54}H_{18}$ with a curvature of the (10,10) SWCNT. We have also used a flat carbon flake to simulate a nanotube of very large diameter. The results show that Pt clusters bind to the carbon structure creating multiple connections. The binding is rather weak and the Pt cluster can migrate on the carbon surface much more easily than H atoms: the estimated barrier for the axial migration of Pt_4 on a CNT is much lower than for the radial mobility (0.3 eV versus 1.6 eV). Particularly, the mobility of the Pt_4 on the carbon surface involves more energy cost when the tip of the cluster is down (~ 3 times higher) than for the case in which the tip is up. This is in agreement with the periodic model calculations reported earlier.

We have also studied the behavior of the Pt_4-$C_{54}H_{18}$ system with an H_2 molecule attached to the Pt cluster. Our calculations show that in such a case the platinum reduces the number of connections to the carbon surface and reorients itself in such a way that H atoms are closer to the carbon surface (see Figure 5). Also, such a system behaves slightly differently when the carbon surface is either flat or bent (different diameters of CNTs).

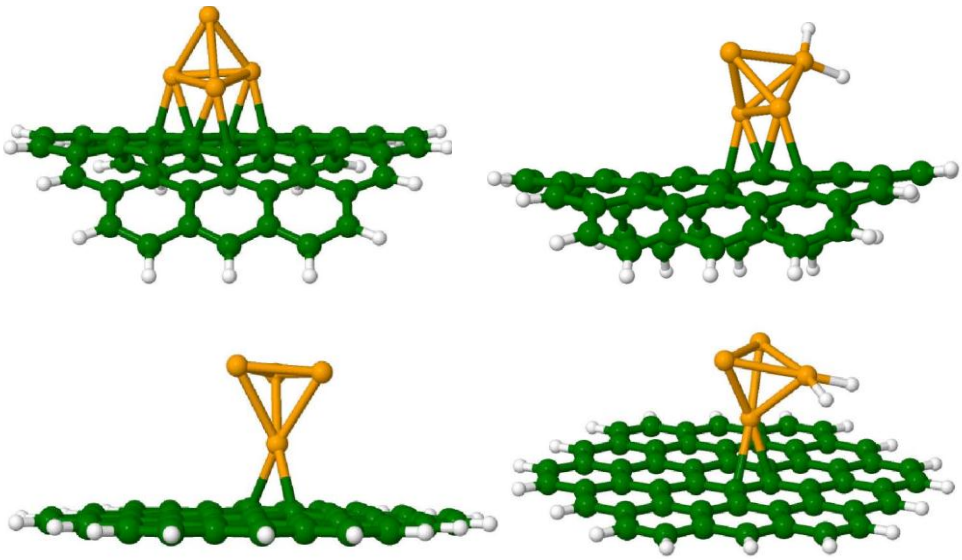

Figure 5. Optimized structures of Pt_4 (left panel) and Pt_4-2H on the (right panel) planar and bent C54H18 structure.

In the case of a flat carbon substrate the H atoms on the Pt cluster are oriented parallel to the carbon surface and the spillover to the substrate seems to be more facile.

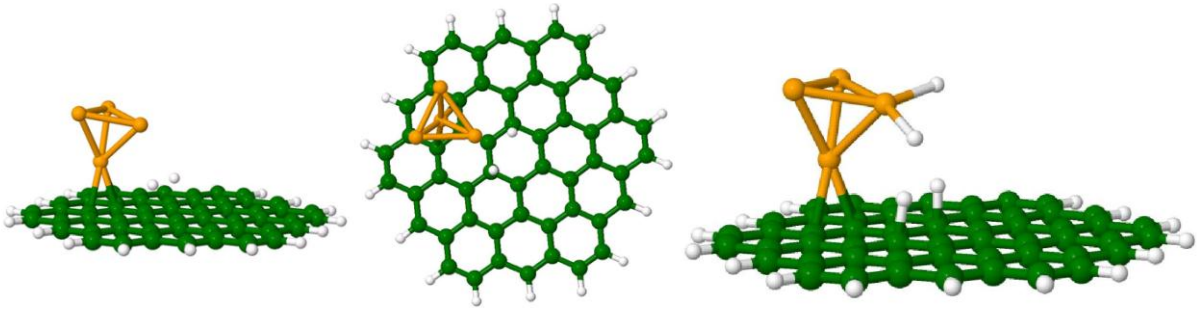

Figure 6. Proposed mechanism of the H atom spillover from a Pt cluster to the carbon substrate. (left and middle) first step shown from the side and the top with two H atoms being moved to the carbon and (right) second step with another two H atoms being introduced.

The calculated average activation barrier for the H migration from the fully saturated Pt_6 (Pt_6H_{24}) has been reported in the literature to be 0.48 eV per H atom onto a graphene sheet.[35] These calculations have been performed using the PW91 exchange-correlation functional.

The Pt clusters seem to be more mobile on the carbon substrate in agreement with the periodic model calculations and they can easily dissociate H_2 molecules; this is an important part of the spillover mechanism. The calculated barrier to hydrogen transfer from the cluster to the SWCNT substrate is low enough (0.48 eV)[35] that hydrogen spillover can occur as recently observed experimentally.[36] Hydrogen storage through spill-over mechanism is studied in 1:1 porous carbon nitride nanotubes. The hydrogen gravimetric density is calculated to be 3.7 wt%.[37]

Deliverable D3.14: Progress report on H atom diffusion and recombination over SWCNT

The objective is to investigate the process of hydrogen diffusion and recombination on the single walled carbon nanotubes (SWCNT) surface. This process determines the lifetime of hydrogen storage systems on the basis of SWCNT, as an undesired recombination would result in H_2 release, and hence in aging of the storage device. We will investigate this process using classical and quantum-mechanical theories.

The work on this Deliverable is having two Objectives: The diffusion of H on SWCNT is important for the spillover-based loading and unloading of the SWCNT. In order to achieve technologically interesting loading and unloading times, the diffusion rate needs to be in the order of micrometer per second. On the other hand, the recombination rate of two H atoms attached at neighboring lattice sites must be small in order to maintain a long-term storage (in the order of days at room temperature). Both numbers are very sensitive to the environment, in particular concerning the presence of traces of catalysts.

(i) Investigation of hydrogen diffusion on SWCNT

The possible pathways of hydrogen diffusion in the configurations were studied and the possible mechanisms for the diffusion examined. All pathways studied were found to be associated with high barriers, with the lowest barrier for diffusion found to be 2.22 eV. This suggests that the diffusion of hydrogen over SWCNT is a highly unlikely process. It remains to be investigated to what extent quantum phenomena (tunneling) can play a role in this process, however, at this stage the mobility appears to be too low for a technological device based on hydrogen diffusion but, *e.g.* diffusion of metal particles to deposit and release hydrogen is thus a more likely process.

(ii) Investigation of hydrogen recombination on SWCNT
The second part of this work, which involves the recombination of two H atoms, which are bonded next to each other on a SWCNT, is now less likely to be relevant. Instead the experimentally observed hydrogenation of SWCNT decorated with Pt nanoparticles is more likely to be explained by spillover of atomic hydrogen deposited by mobile metal clusters on the SWCNT.

(iii) Results for hydrogen adsorption on a carbon flake with a curvature of the (10,10) SWCNT
We have studied the adsorption of H atoms on the carbon surface of a model $C_{54}H_{18}$ structure. The results show that two H atoms prefer to adsorb on the carbon surface in the position para or ortho (only 0.18 eV less stable than para), while position meta is by 1.24 eV less stable. This is in agreement with the work of Lin et al., where the authors show that two H atoms attached to the same hexagon prefer either para or ortho positions, while the meta position is much less attractive.[38] Also, the energy necessary to attach another two H atoms to the carbon surface is much lower than in the case of the first pair of H atoms. Energy is reduced if π-bonds of the carbon surface are transformed into sp^3 bonds in the same ring first and then in the adjacent rings.

Moreover, Chen et al. have studied the diffusion of H atoms on graphene and carbon nanotubes.[35] The activation energy for the diffusion of H between two adjacent sites is 1.42 eV on (5,5) and 1.09 eV on (9,9) SWCNT, respectively. The lowest activation energy was found for the graphene layer (0.78 eV). This is still more than a factor two higher than the energy of Pt_4 diffusion calculated in our model system (0.3 eV). We can conclude that it is more likely that during the spillover mechanism Pt clusters dissociate the H_2 molecule into atoms which are later migrated to the carbon surface and then the cluster moves away to repeat the process in another place of the SWCNT. This is in very good agreement with our previous calculations on the periodic CNT. This also confirms the validity of our finite model calculations.

(iv) Recombination of H atoms from the carbon surface
Pt cluster support is crucial to recombine the H atoms from the carbon surface to form an H_2 molecule. The energy barrier without Pt is very large (around 3.1 eV) for such a process (see Figure 7).

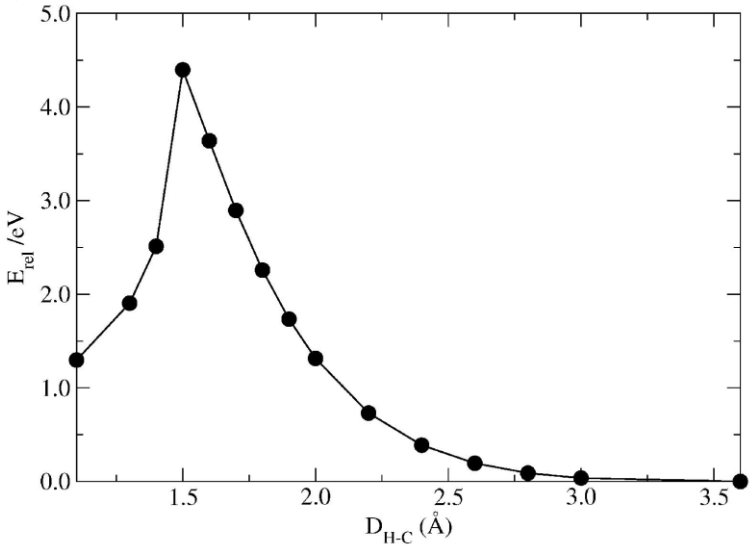

Figure 7. Barriers for the recombination of H_2 molecule without Pt_n cluster.

The mechanism of H diffusion on SWCNT has been investigated and will be published together with the results of D13. While potential quantum effects might slightly alter the preliminary conclusions – our simulations indicate a very low mobility of H on CNT. The recombination of two H atoms at

neighboring sites is unlikely and the involvement and active role of mobile Pt nanoclusters on the SWCNT in depositing and releasing hydrogen will be investigated.

Deliverable D3.15: Progress report on requirements for use of H-covered SWCNT as proton releasing electrode

The objective is to investigate whether H-decorated SWCNT's can be directly employed as electrodes in a fuel cell catalytic process. The vision is to build a system where a cartridge of H-covered SWCNT's, when spent, is replaced by another cartridge such that a minimum effort is required by the user on the recharging of the fuel cell capacity.

The work has been performed in close collaboration with the experimental group headed by Anders Nilsson, Stanford University, who has performed ground-breaking studies of hydrogenation of carbon nanotubes initially using predissociated atomic hydrogen to fully hydrogenate the nanotubes.[39] In a second step the nanotubes were partially decorated with Platinum and spillover of hydrogen onto the nanotubes was demonstrated.[36]. Studying this process formed WP D13 of the present project. Controlling the amount and dispersion of the Platinum particles on the nanotubes turned, however, out to be experimentally too challenging for the moment since a "forest" of nanotubes had to be grown on a conducting substrate where the nanotubes should be decorated with Pt nanoparticles in a controlled way and this path was abandoned. On the other hand, it is well-known that it is the oxygen-reduction reaction at the cathode which is rate-limiting in fuel cell catalysis and here our experimental partners had made a new break-through by demonstrating that dealloyed Pt_3Cu nanoparticles showed significantly higher reactivity than Pt.[40] Dealloying results in a Pt-rich surface shell with a Cu-rich core which generates a strain on the exposed Pt atoms since the lattice is closer to that of Cu than Pt. A series of combined experimental and theoretical studies were initiated to follow up on this exciting possibility to reduce the amount of Pt needed at the cathode while also enhancing the rate in fuel-cell catalysis. We have thus concluded that, at least with the present resources the original idea with reloadable cartridges acting as electrodes in the fuel cell is not feasible. Significant work has instead been put in on the other electrode in the process where the oxygen-reduction reaction takes place. This will be described below.

Complementarity between high-energy photoelectron and L-edge spectroscopy for probing the electronic structure of 5d transition metal catalysts.[41]

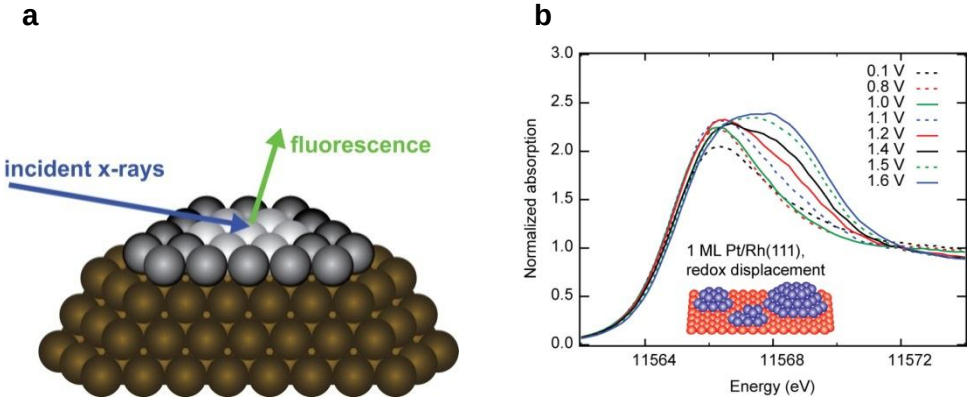

Figure 8. (a) Schematic illustration of x-ray spectroscopy probing of a single monolayer of Pt on top of Rh(111) using grazing incidence of the incoming x-rays, (b) Pt L3 edge HERFD XAS spectra of 1ML Pt/Rh(111) in 0.01M HClO4 as a function of increasing potentials.

Figure 8a shows how a Pt single monolayer can be probed on single-crystal surfaces. This method allows the intrinsically bulk sensitive hard x-ray spectroscopy to probe only surface atoms that are in direct contact with the electrolyte. By adjusting the incidence angle to the critical angle for total external reflection, the signal from the top few monolayers is further enhanced. Figure 8b shows the L-edge x-ray absorption spectra (XAS) of a Pt monolayer on Rh(111) detected using High Energy Resolution Fluorescence Detection (HERFD), where the life-time broadening of the Pt L-edge has been experimentally removed, resulting in much higher resolved spectral features. By using the L_3-edge, the unoccupied Pt 5d-states are probed. The intensity increase, broadening, and shift of the spectra with increasing potential were identified, through theoretical spectral simulations, to result from the development of a Pt surface oxide. Complementary extended x-ray absorption fine structure (EXAFS) measurements have been carried out under identical conditions. Pt-Pt and Pt-O bond lengths and coordination numbers have been derived, confirming the interpretation of the growth of a surface Pt oxide on the model catalyst. Weaker changes in the spectral features at lower potentials can be related to adsorbed hydrogen and to the presence of other oxygenated species. Figure 9 shows a summary of the potential-dependent surface coverages of two different Pt/Rh(111) electrodes. FEFF calculations were used to identify the spectral signatures of various surface species. The two different surface preparations result in either a uniform two-dimensional (2D) monolayer or three-dimensional (3D) islands as indicated in the figure. What is most interesting is that these two surfaces respond very differently to the applied potential when exposed to H_2 and O_2. For the 3D Pt islands we see 4 different regions of adsorbed H, O/OH, Pt oxide or surface without strongly adsorbed species, whereas for the 2D Pt layer we only observe either Pt oxide or a metallic, adsorbate-free Pt layer but neither adsorbed H nor O/OH. The spectral changes induced by O and OH are very similar, so it has not yet been possible to distinguish these two cases. The reason for this difference in reactivity is that the Pt in direct contact with Rh is modified to such an extent that it does not bond H and O/OH strongly enough. This is the first time that the various surface species could be mapped during *in situ* conditions of the oxygen reduction reaction albeit on a relatively simple model system.

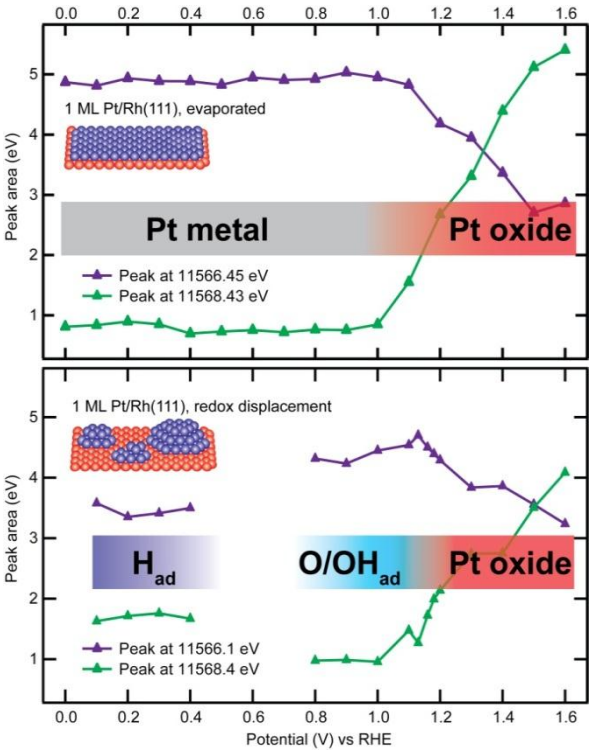

Figure 9. Potential-dependent evolution of the HERFD XAS white-line shape for two different Pt/Rh(111) model electrocatalysts, measured *in situ* in 0.01 M $HClO_4$. The white-line can be fitted with two Gaussian functions, whose intensities are plotted as function of increasing potential. The observed changes can be attributed to an adsorbate-free or H_2O-covered Pt monolayer, chemisorbed H, chemisorbed O/OH and Pt oxide, as indicated in the graphs.

Figure 10 shows both XPS of the Pt substrate oxygen atoms as well as O K-edge polarization-dependent XAS for the different states of the Pt surface under a few mbar of O_2 gas at elevated temperatures.[42] Based on the XPS spectra a model of the surface could be proposed which was further tested using spectrum calculations of the XAS data. We could identify several chemisorbed phases of oxygen and two different classes of Pt-oxides, a surface PtO-like oxide and a layer of PtO_2, depending on pressure and temperature. Using different exposures to hydrogen we could clearly demonstrate that it is the chemisorbed phase and the PtO_2 that can be reduced whereas the PtO surface oxide is rather inert towards hydrogen. These results are consistent with recent findings regarding the ORR reaction on Pt(111) using *in situ* hard x-ray spectroscopy as described above, where the reduction of Pt oxide could become rate limiting at high potentials. It is clear that with ambient pressure XPS in combination with theoretical DFT simulations of spectra a lot of details regarding surface composition and intermediate adsorbates under *in situ* conditions can be obtained.

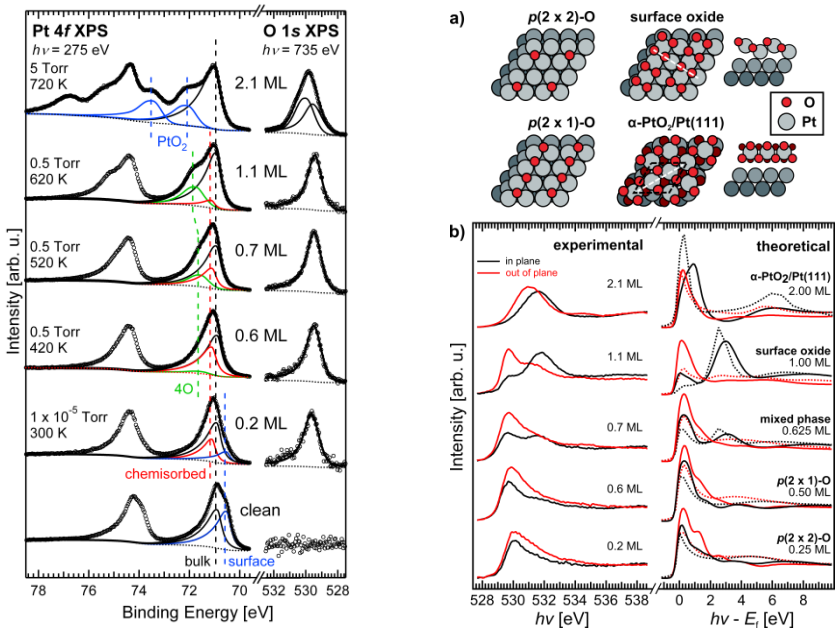

Figure 10. (Left) Pt 4f and O1s XPS spectra of Pt(111) in different O_2 gas pressures and temperatures. (Right) a) Proposed structure models of O/Pt(111), b) experimental and simulated O K-edge spectra based on the structural models in a).

Oxygen dissociation on Pt(111) electrodes. The kinetic behavior of the dissociation of O_2 at saturation coverage is consistent with a very high barrier to dissociation within compact superoxo clusters, which almost entirely cover the surface under these conditions. DFT calculations indicate that dissociation is highly activated (E_a = 0.76 eV) within dense O_2 islands, where the coverage can locally reach 0.5 ML; in contrast desorption is observed to be facile (E_d = 0.32 eV). The dissociation of a saturated adlayer is thus strongly inhibited until the onset of desorption at 110 K generating empty sites that can be occupied by dissociated atoms.

The most favorable sites for dissociation may not, however, lie in locally adsorbate-free regions of the surface, but rather in the vicinity of adsorbed atomic oxygen or within disperse O_2 phases. Crucially, DFT barrier estimates do not decrease monotonically as the total oxygen coverage is reduced: the lowest computed barrier (0.24 eV) is obtained using the (2√3 × 2) supercell shown in Figure 11, despite the high local coverage of 0.25 ML. We attribute the low barrier obtained in this case to attractive O–O interactions at two lattice spacings ($2a_{NN}$) that strongly stabilize the atomic final state. These lateral interactions rapidly decay beyond $2a_{NN}$, whereas at $1a_{NN}$ and $\sqrt{3}a_{NN}$ they take on a highly repulsive character. We accordingly find that the atomic binding energy decreases as we expand the supercell size to (2√3 × 3) and (2√3 × 4). Similarly, reducing the supercell size to (√3 × 2) weakens the atomic binding energy by up to 0.5 eV/atom compared to the favorable (2√3 × 2) case and produces a concomitant 0.5 eV increase in E_a, which accounts for why aggressive oxidizing conditions are required to induce dissociation beyond θ = 0.25 ML.

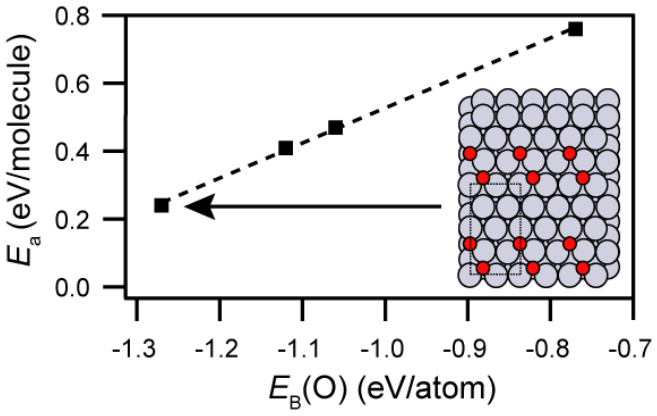

Figure 11. Computed O_2 dissociation barriers (E_a) for ($\sqrt{3} \times 2$) and ($2\sqrt{3} \times n$) (n = 2, 3, 4) supercells plotted against atomic binding energies (EB(O)). The dashed line is a fit to the data: Ea follows a linear Brønsted-Evans-Polanyi relationship. (inset) Atomic final state of O_2 dissociation for the ($2\sqrt{3} \times 2$) supercell (θ = 0.25 ML) indicated by the dashed rectangle.

Variations in the final atomic binding energy are reflected in the dissociation barriers, which follow a linear Brønsted-Evans-Polanyi relationship, as illustrated in Figure 11. We postulate, therefore, that attractive final-state interactions favor dissociation either at the edges of atomic *p*(2 × 2) islands or chains, or within disperse O_2 phases in which molecules are spaced at least $2a_{NN}$ apart. For surfaces initially saturated with O_2, partial adlayer desorption allows dissociation to occur by creating localized regions of reduced adsorbate coverage. The prediction of enhanced oxygen reactivity at the edges of growing *p*(2 × 2)-O phases helps to rationalize the very low barrier measured at saturation; indeed, the experimental barrier of ~0.27 eV is in excellent agreement with the theoretical estimate of 0.24 eV for the (2√3 × 2) supercell. Analogous lateral effects were also invoked by Ertl and coworkers to account for the extended *p*(2 × 2)-O chains that form when oxygen gas is dosed onto Pt(111) between 95 and 115 K.[43]

To conclude, detailed kinetic XPS measurements yield a very low barrier of 0.27 eV for O_2 dissociation on Pt(111). A particularly important finding is that DFT reproduces this low barrier *if* specific adsorbate-adsorbate interactions are taken into account: attractive third-nearest neighbor interactions give rise to a computed barrier of 0.24 eV at 0.25 ML. Additionally, we have shown that estimates of 0.80 eV or more for E_a based on small supercells are not artifacts, but rather are consistent with the stability of saturated O_2 adlayers below the onset of desorption. We propose that the inclusion of adsorbate-adsorbate interactions is essential in general when modeling catalytic reactions at surfaces, especially under conditions that favor high-coverage adsorbate phases, for example at electrochemical interfaces or elevated gas pressures. Adsorbate-adsorbate interactions could for instance play an important role in ORR, since O_2 dissociation is likely to be affected by the presence of O, OH and H_2O species at the catalyst surface.

Strain and alloying.In order to investigate the electronic structure of the oxygen adsorbate as it couples to the metal substrate of the dealloyed Pt@Cu catalyst we employed O *K*-edge XES and XAS, which provide atom-specific information about the valence states projected onto the excited atom. A complication here is that atomic oxygen binds more strongly to copper than to platinum which makes it necessary to consider alternative surface compositions than the desired exposing Pt and having Cu as support; when oxygen binds to the surface it may cause Cu to segregate to the surface. The experimental model system was 1-3 ML Pt on Cu(111) but in the simulations we had to consider

all possible relative abundances of Pt and Cu at the surface within the (limited) unit cell used.[44] Only then could the spectra be accurately reproduced and interpreted.

Figure 12a shows, on a common binding-energy scale, experimental oxygen *K*-edge XES and XAS spectra of oxygen chemisorbed on Pt(111) and the different Pt/Cu(111) systems.[44] The experimental binding energy scale was obtained by subtracting the O 1*s* XPS binding energy from the excitation and emission photon energy scale for XAS and XES spectra, respectively. Figure 12b shows calculated XAS and XES spectra of O-Pt(111). To model the strained system spectra for the 9 model systems with the lowest total energy were weighted together by a least-squares simultaneous fit to experimental XES and XAS spectra for the best agreement; the model systems included all possible arrangements of four Pt and four Cu atoms in the first two layers. Also, the spectra of O adsorbed on unsegregated Pt/Cu(111), *i.e.* exposing only Pt, is shown as a reference. The experimental spectra are included in Figure 10b to facilitate comparison.

The p_{xy}- and p_z-projected XES spectra of the systems in Figure 12a exhibit two broad structures attributable to oxygen-derived bonding and antibonding states. For the O/Pt(111) reference system, the p_{xy}-projected bonding and antibonding states are located 6 and 2 eV below the Fermi level, respectively, whereas the corresponding p_z-projected peaks are further broadened and reside ~5 and 1 eV below E_f. This shift of the p_z states to lower binding energy appears to be a general trend for atomic adsorbates on metal surfaces. The bonding states exhibit greater XES intensity than the antibonding states, which indicates that the former are more of oxygen character and the latter of metal character. Moreover, XAS indicates that the antibonding states spill over the Fermi level and are therefore not fully occupied. Note that the relative intensity scale between the XAS and XES spectra is arbitrary such that the relative population of antibonding (XAS) and bonding states (XES) cannot be simply concluded from the figure.

Turning to Figure 12b we compare the symmetry-resolved theoretical and experimental spectra for the O-Pt(111) system, bottom set, and the theoretical estimate to the 1.1 ML O-Pt/Cu(111) system, top set. Starting with O-Pt(111), we note that both in XES and XAS the overall agreement is very good, and although the calculated XES spectra are slightly broader, the observations from Figure 12a remain when considering also the theory. The top set of spectra compare measurements for the 1.1 ML O-Pt/Cu(111) system with the least-squares fit of calculated XES and XAS spectra (red) for the nine most stable (energies within ~0.4 eV) structures including adsorbate-induced segregation. In addition, we show computed spectra for oxygen on 1ML of strained Pt on Cu(111), blue spectra in Figure 12b.

Focusing on the XAS we note in the p_{xy} resolved spectra a good agreement for the fitted spectra with the experiment where no pronounced peak, but rather a shoulder, arises above E_F. To compare, the computed pure monolayer spectrum resembles that of O on Pt(111) where the pronounced peak in the O 1*s* XAS near E_f indicates a larger involvement of Pt in the adsorbate-substrate bond compared to O-Pt/Cu(111). Also in the p_z XAS, the intensity of the peak is too pronounced compared to O-Pt/Cu(111), giving strength to the argument of Cu segregation. Turning to the XES, the fitted spectra are in very good agreement with the experiment. And also here, by noting the significantly broader features of the unsegregated O-Pt/Cu(111) spectra, which rather resemble the O-Pt(111) system, we conclude that Cu segregation into the top layer is required to reproduce the features in the experimental spectra.

Since the antibonding states of O/Pt(111) cross the Fermi level, downshifting the *d*-band should intuitively weaken the surface–adsorbate chemical bond by pulling the antibonding states below the Fermi level, hence increasing their occupation. Observing the spectra in Figure 12a, the peak attributed to the O derived antibonding states becomes, most obvious for the p_z spectra, more pronounced with increased compressive strain.

These arguments could rationalize the observed trends for oxygen adsorption on Pt/Cu(111) since the valence-band XPS shows that both compressive strain and ligand effects tend to lower the Pt 5*d*-band of the overlayers with respect to that of pure Pt, which in turn would lead to an increase in the filling of the metal *d*–O 2*p* hybridized antibonding states. A similar effect was observed for the XES and XAS spectra of N adsorbed on Ni(100) and Cu(100). There, N-projected N 2*p*–Cu 3*d* antibonding states were observed to be below the Fermi level for Cu(100), but above the Fermi level for Ni(100), the reason being the lower-lying 3*d* band of Cu(100) compared to Ni(100). However, for the present system it becomes more complicated.

In Figure 12a, it is apparent that the coupling of the adsorbate with the metal *d*-band gives rise to O 2*p*–metal *d* bonding and antibonding states located below and above the metal *d*-band, respectively, but by looking at merely the adsorbate-derived density of states, the picture is incomplete and would lead to the conclusion that by adding strain the adsorbate-metal bond becomes weaker, which for some systems is true. The severe effect of oxygen-induced segregation results in surface-alloying, which alters the substrate electronic structure considerably. Therefore we need to consider the changes in the metal *d*-DOS upon segregation when discussing properties of the oxygen-substrate bond in this system.

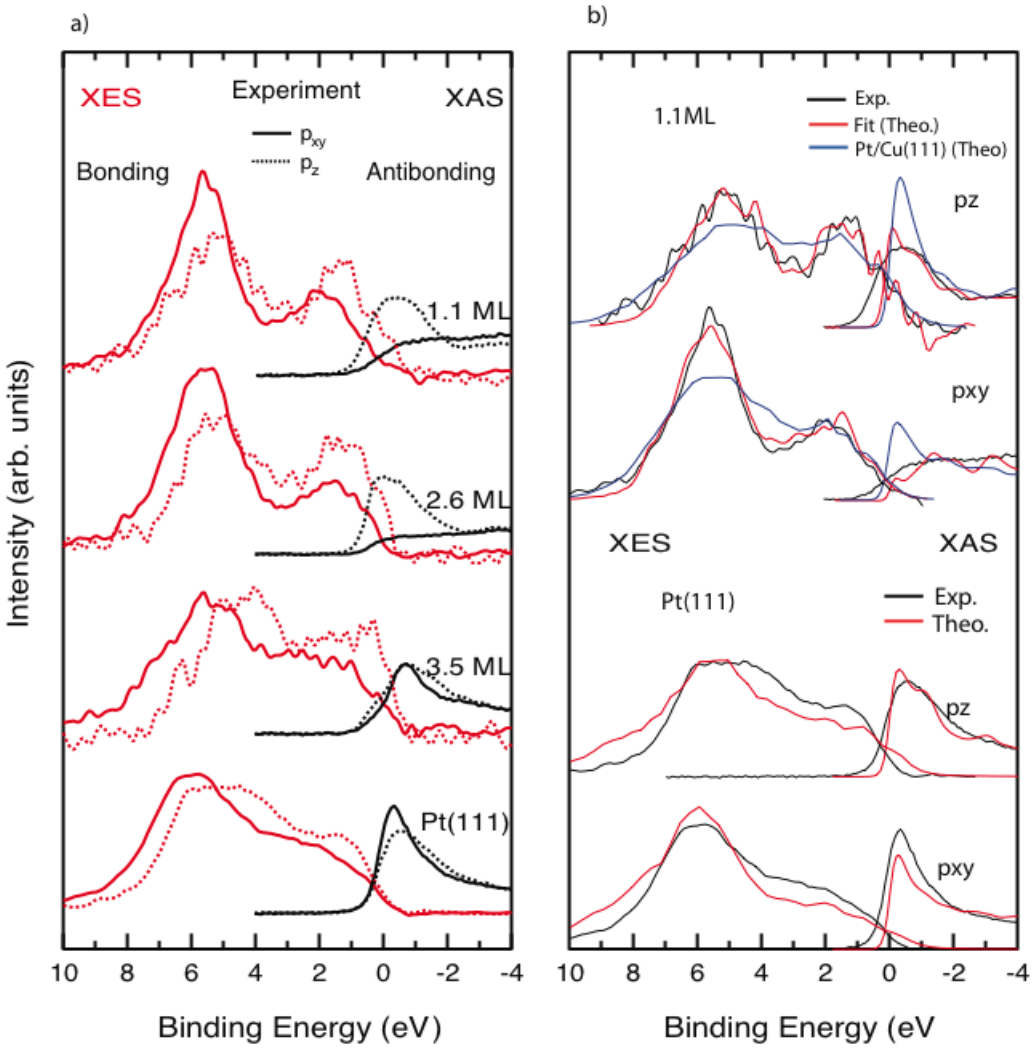

Figure 12 a) Oxygen K-edge XES (red lines) and XAS (black lines) of atomic oxygen chemisorbed on pure Pt(111) and on various Pt/Cu(111) samples. Spectra related to the pxy adsorbate states are drawn with solid lines and those related to pz are drawn with dotted lines. The XAS spectra are normalized to the same step height well above the absorption edge; the scaling between XES and XAS spectra is, however, arbitrary. b) Calculated O K-edge XES and XAS compared to chosen spectra from 5a), O-Pt(111) and O-Pt/Cu(111) 1.1ML. Bottom set shows experimental (black) and calculated (red) pz adsorbate states above the pxy resolved spectra of O on Pt(111). Top set shows the measured O-Pt(1.1ML)/Cu(111) pxy and pz spectra (black) compared to spectra obtained from the segregated structures, see main text, least square fitted to the experiment (red) as well as calculated spectra for the O-Pt/Cu(111) structure (blue).

Deliverable D3.16: Database of hydrogen storage capacities (gravimetric/volumetric) for nanoporous materials as function of pressure and temperature

Explicit calculations on different systems at various temperature (T) and pressure (P) are carried out. Temperature – pressure phase diagrams are generated through the study of hydrogen adsorption on the $(N_4C_3H)_6Li_6$ cluster at the B3LYP/6-31+G(d) level of theory. Possibility of hydrogen storage in an associated 3D functional material is also explored.[45]

Deliverable D3.17: Understanding of quantum effects

The objective of this part of the work was to investigate the role of quantum effects on the adsorption of molecular hydrogen in framework compounds. We have shown that the differences

between classical and quantum mechanical computer simulations are significant, surprisingly even at room temperature, in case of hydrogen gas trapped in small pores.

Hydrogen storage by physisorption is targeted – at present – to systems that are cooled by liquid nitrogen. At that temperature, the de Broglie thermal wavelength of hydrogen molecules (Λ = 1.40 Å) is close to the critical value (Λ_c = 1.48 Å) for the breakdown of the approximation in the uniform system. Therefore, we investigated[46] the performance of a classical simulation (here, no quantum effects are applied to hydrogen) with that of two quantum mechanical simulations. The first employs Maxwell-Boltzmann statistics, as usually done for Quantized-Liquid Density Functional Theory (QLDFT),[1] and the second the recently implemented and physically correct Bose-Einstein statistics. We find that there is a large difference between classical and quantum simulations, and even find strong deviations for systems with small pores at temperatures as high as 300K. On the other hand, no difference is found between Bose-Einstein and Maxwell-Boltzmann statistics for temperatures as low as 50K. The simulations have been carried out on carbon foam model systems, an example for room temperature (T=300K) is given in Figure 13.

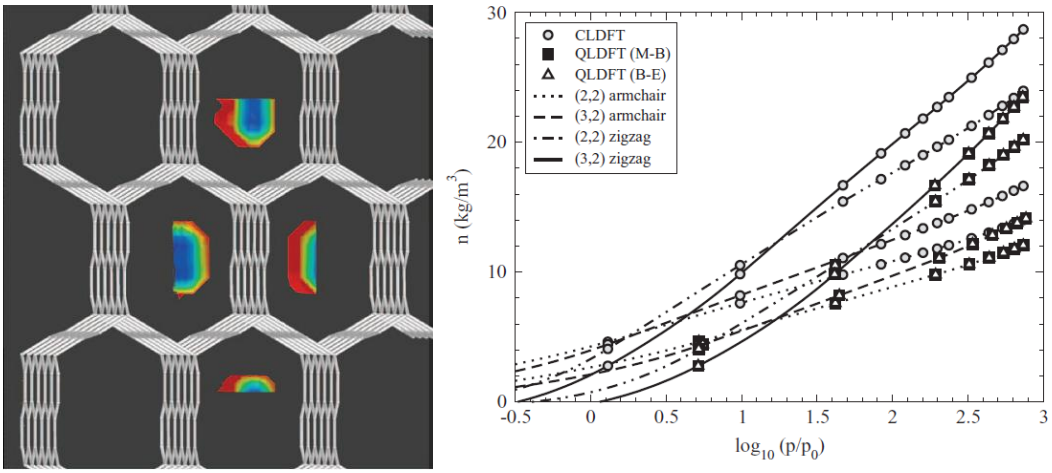

Figure 13. (Left) Hydrogen density adsorbed in a (2,2) armchair carbon foam. The hydrogen density (red: large density, blue: small density) is shown in the area covered by the simulation box. (Right) Hydrogen uptake, depending on pressure, for different carbon foams at 300 K, calculated using QLDFT. For details, see the article by Heine et al.54

In conclusion, quantum effects are indeed important for all computer simulations that study hydrogen physisorption in nanoporous materials.

Deliverable D3.18: Understanding of properties of nanostructured materials with chemi- and physisorption properties

A considerable improvement on hydrogen storage can be achieved if a porous material can both chemi- and physisorb hydrogen. For example, metal centers or metal clusters, incorporated in a framework material such as metal organic frameworks or porous carbon compounds, could activate the hydrogen and form metal hydride clusters. At the same time, the skeleton of the framework acts as host for physisorbing more hydrogen gas. Following basic chemical principles (Le Chatelier), the reversible physisorption process could be controlled over the pressure (and hence the amount of physisorbed hydrogen) in the sample.

Metal hydrido-amine complexes (metal = Ru, Rh, and Ir) attract ever increasing attention as highly active and enantioselective transfer hydrogenation catalysts. The key feature of most transfer hydrogenation catalysts is the presence of a hydridic M-H subunit adjacent to a protic N-H functionality. In neutral and basic conditions the catalyst transfers these two hydrogen atoms to polar unsaturated substrates, avoiding direct coordination of the substrate to the metal. As a consequence of this hydrogen transfer, the catalyst is converted into a 16-electron amido entity through a six-membered ring transition state 2. Then, in the catalyst regeneration step, dihydrogen sources provide H_2 to the amido complex to re-form the 18-electron amino-hydride. We investigate[11] by density functional theory (DFT) the mechanistic details of the overall reaction of the iridium transfer hydrogenation catalyst Cp*Ir(TsDPEN-H) with H_2 and O_2 with the support of the experimental observations and the proposed reaction mechanism. We believe this work could contribute to enhance further understanding and provide helpful information that would inspire the design of new catalysts for fuel cells.

The mechanistic details of the reaction that occurs in the fuel cells between oxygen and hydrogen in the presence of catalysts were studied by using first principles methods. In particular, the hydrogenation of molecular oxygen by the 18e amino-hydride Cp*IrH(TsDPEN) (1H(H)) complex to give Cp*Ir(TsDPEN-H) (1) and 1 equiv of H_2O were investigated by means of hybrid density functional calculations (B3LYP). To describe the overall catalytic cycle of the hydrogenation of dioxygen using H_2 catalyzed by the Ir complex 1, the potential energy surfaces for the hydrogenation process of both the catalyst 1 and the corresponding unsaturated iridium(III) amine cation ([1H]+) were explored at the same level of theory. The results of our computations, in agreement with experimental findings, confirm that the addition of H_2 to the 16e diamido complexes 1 is favorable but is slow and is accelerated by the presence of Brønsted acids, such as HOTf, which convert 1 into the corresponding amine cation [1H]+. By deprotonation of the subsequently hydrogenated [1H(H_2)]+ complex the amine hydride catalyst 1H(H) is generated, which is able to reduce molecular oxygen. Preliminary results concerning the O_2 reduction in acidic conditions show that the reaction proceeds by intermediate production of H_2O_2, which reacts with 1H(H) to eliminate water, restore [1H]+, and restart the catalytic cycle. The energetics of the process appear to be definitely more favorable with respect to the analogous pathways in neutral conditions.
Furthermore, the possible release of H_2 from reactions of HUO_3 ions with CH_3OH substrates has been considered. The reaction is thermodynamically exothermic and the energetic barriers necessary to produce H_2 lie below the reactant energies.
In conclusion, the idea to combine chemisorption and physisorption remains a valid one. Its realization crucially depends on the progress in synthetic methods that would be able to incorporate reactive metal atoms and clusters into framework materials. A promising route has been recently suggested in silico, where MOFs with halogenated niobium clusters are used as linkers.[47]
Three-dimensional carbon allotropes based on cubane and expanded cubanes were studied for molecular hydrogen storage. These proposed allotropes are found to be highly porous in nature and can adsorb molecular hydrogen with a gravimetric density of ~ 3.0 wt%.[48]

Deliverable D3.19: Database of diffusion constants of various gases in nanoporous materials

The database is currently compiled by our Indian partners. Once finalized, it will be made available to the general public on the project website.

WP4: Improving fuel cell performance by increasing conductivity

Proton exchange membranes as electrolytes have advantages, yet suffer from low mechanical, thermal and chemical stabilities. This highlights the importance of new polymeric designs which overcome the present instabilities. The proton diffusion mechanism of azole derivatives and their

solvent effects were theoretically studied in D4.20. This deliverable finished on time and resulted in proposing a new mechanism for proton conduction in polymers. Databases of proton diffusion rates in sets of high temperature membranes (D4.21) and ceramic materials (D4.22) have also been prepared and made available in the project website for the general public. Essential guidelines for the design of new protonic ceramics and polymers are narrated in D4.23.

Deliverable D4.20: Chemical insights on the role of the different chemical and environmental effects on the proton diffusion mechanism

Methods rooted in Density Functional Theory have been applied to study the proton transfer reaction in imidazole-based polymers, which are solid electrolytes used in Proton Exchange Membrane Fuel Cells (PEMFCs). In particular, imidazole, triazole and tetrazole based systems, presenting a large range of proton conductivity rates, have been considered in order to give insights on the nature of chemical and environmental effects on the proton transfer mechanism. Our results showed that the energetics of the proton transfer is very similar in these systems. However, the rate determining step is the imidazole rotation to restore the initial conditions which means that less substituted cycles could give better conductivity.

As a first step, a DFT computational approach has been developed to analyze, from a quantitative point of view, the energetic features of proton transfer reactions in simple model systems, including a protonated imidazole dimer. Indeed such systems represent the smallest model of the imidazole-based solid electrolytes used in PEMFCs. The computational approach is based on an improved exchange-correlation functional giving accurate proton transfer (PT) energetic barriers and it has been used to compute thermodynamic and kinetic features of several PT reactions.[4]

Then, other models systems, namely 1,2,3-triazole, and tetrazole dimers have been considered. These molecules are among the most promising basic constituents of new polymeric membranes. The aim was to elucidate the experimental differences in proton conduction between these molecules and the reference imidazole and rationalizing their behavior in terms of the chemical structure (electronic effects).[49] Another important point was to characterize the most probable (in terms of energetics) mechanism in 1,2,3 triazoles (2 possible PT mechanisms) or in tetrazole dimers (3 possible PT mechanisms) and to compare experimental and theoretical hypotheses on proton conduction. From a more computational point of view, a not less important aim was to determine the most suitable approach for this family of molecules, both in terms of structure and energetics, in view of applications to large systems.

Finally, the constraints imposed by the insertion of the imidazoles in a polymeric backbone were analyzed. Indeed the polymer strongly affects the flexibility of the imidazole chain, leading to higher barriers for proton conduction. A further modulation is then represented by the solvent (environmental) effects, modeled as a continuum dielectric.

Our simulations showed that the transfer of several protons from one end to the other of the polymers is direct as in the free imidazole pairs, but it is coupled with the rotation of the dangling imidazoles, needed to restore the initial conditions after the first PT. Indeed this rotation is the rate-limiting step and, therefore molecules with lower steric hindrance at the atom close to the polymer backbone, should provide better conductivity.[50] The work has been carried out in strong connection with partner 2 (ENSCP-CNRS).

The main outcome concerns a detailed analysis of the chemical effects on the proton transfer mechanism in the considered azole-derivatives and the proposition of a new mechanism for proton conduction in polymers. These results represent precious insights for the creation of a proton diffusion database (D4.20 and D4.23). This information has been shared with all the partners of the consortium and it has been published in 3 articles in peer-reviewed international journals.

Deliverable D4.21: Database of proton diffusion rates in a series of high-temperature membranes, in dependency on temperature and solvent

The database is available for the general public on the project website.

Deliverable D4.22: Database of proton diffusion rates in a series of ceramic materials, as function of the matrix composition and defects

The database is available for the general public on the project website.

Deliverable D4.23: Hints for the design of new protonic ceramics and polymers

Proton diffusion in the fuel cell membrane is modeled by triflic acid, which is the simplest model for the active site of Nafion. Results obtained from static calculations show that a minimum of three water molecules is required to conduct the proton.

Proton transfer in monoprotic carborane derivatives has been studied with a view to design new fuel cell membranes. Results obtained from the calculations highlights that these derivatives can be useful in proton exchange membrane fuel cell applications.[51]

A detailed calculation is carried out to determine the structure, stability, and reactivity of $B_{12}N_{12}$ clusters with hydrogen doping. Related cage aromaticity of this $B_{12}N_{12}$ and $nH_2@B_{12}N_{12}$ is analyzed through the nucleus independent chemical shift values.

Hydrogen binding ability of various gas phase stable dianionic species, $B_nX_n^{2-}$ (X = BO, CN, NC; n = 4-12) and their carbon doped analogues are theoretically tested. Some 3-D networks are also designed in this regard. Each O, N, C center is found to bind with three molecular hydrogens at the studied levels of theory with reasonably good interaction energy per hydrogen molecule.

A computational study is made to explore the structure, stability and hydrogen storage capacity of three $C_{12}N_{12}$ cage isomers and we find that all the three isomers can bind up to 12 H_2 molecules. The hydrogen binding energy can be significantly improved by applying an external electric field. Determination of their gas phase heat of formation through schematic isodesmic reaction indicates these materials as probable high energy density materials.[52]

Please provide a description of the potential impact (including the socio-economic impact and the wider societal implications of the project so far) and the main dissemination activities and the exploitation of results. The length of this part cannot exceed 10 pages.

Impact

Scientific impact: The publication in high-impact journals and the dissemination of the results at scientific conferences had a high impact on the scientific community. We can state that the methods developed in HYPOMAP are used by the consortium and by others, that the papers are read and cited, and that the information available at the website in form of databases is accessed.

Education of young scientists: Several training activities, such as the workshops organized along the 6 months meetings, external training workshops and summer schools, courses within the local graduate programs have contributed to train the fellows that have been enrolled by the HYPOMAP project to become excellent scientists.

Academic degrees: At the European partners, 2 PhD theses have already been concluded within the HYPOMAP project. 3 further PhD defenses will take place in 2012 and beginning of 2013, where results obtained within the HYPOMAP project constitute an important contribution.

Creation of an inter-European network: The collaboration between the European network partners increased strongly during the network. Complementary expertise has led to sustainable scientific collaborations also in other fields.

Creation of an Indo-European network: Collaboration with India is a challenging target due to different scientific infrastructure, different culture, and different standard of living. Still, a sustainable collaboration culture has been developed and is still active. The collaboration will remain fueled by the fact that many Indian partners have still not received their budget and will continue to carry out research on the project.

Impact on career of PI: The two coordinators of the Indo-European project got locally promoted. HYPOMAP was one of the activities that supported that development.

Dissemination activities

Project website: The project website (https://www.jacobs-university.de/ses/theine/projects/HYPOMAP) hosts relevant information on the project, such as a general description of hydrogen storage and fuel cells for the general public as well as a detailed description of objectives to the scientific community. The website also includes information about the consortium and contact details to the principal investigators. The list of publications of the consortium can be found here, and if access is granted one can download the articles directly from the publishers. At the end of the project, we made the databases of proton conductivity and hydrogen storage capacities publicly available by uploading them to the website. The website will remain online, so the databases will continue to be available to the general public as well as to the scientific community.

Scientific publications: To date, the consortium published 48 articles in international peer-reviewed journals in the context of HYPOMAP. Further publications are in preparation or in the peer-reviewing process.

Participation in conferences and workshops: HYPOMAP PI and fellows participated in numerous conferences and workshops and presented the work in oral and poster presentations.

Summer school: A summer school was organized along the M24 meeting in Bremen. 50 participants, among them most young fellows of HYPOMAP, but many other young scientists from many countries of the world, participated in a two-week summer school entitled "Computational Materials Science for the Environment". HYPOMAP PIs have given a total of 8 lectures at the conference.

Web news: Jacobs University included news on the start of the HYPOMAP project on its website. Another web news piece was launched to advertise the related summer school (see above).

Open days: During the 10th anniversary of Jacobs University in October 2011 HYPOMAP research was presented to a public audience, mainly consisting of interested high school students and parents.

Industry fairs: The coordinator (TH) has been invited to present our activities in fuel cell research at the f-cells 2011 industry fair. The presentation included the activities of the HYPOMAP consortium.

Presence in activities and publications of the European Commission: HYPOMAP was represented at the Workshop "Materials Issues for Fuel Cells and Hydrogen Technologies: from innovation to industry" at MINATEC in Grenoble, France (26./27. March 2012). Moreover, HYPOMAP has contributed a major role to the development of scientific software as reflected in the EC publication (brochure) "Modelling Materials".

Exploitation of Results

Exploitable Results: At the Exploitation Strategies Seminar, a fairly exhaustive list of 11 exploitable results was identified and collectively discussed at the seminar. Although good and constructive exchanges took place, there is still a need for further discussions among concerned partners on most of them for better insight and convergence of views as to their full exploitation. The four academic partners, however, have not expressed interest in a commercial exploitation of results of HYPOMAP. Instead, the results have been made publicly available.

The list of exploitable results, as defined during the ESS, and its actual exploitation, is given below.

No	Result	Respon-sible PI	Exploitation
1	Database of analytic host H_2 potentials and parameters	TH	The database is still being refined. Once completed, it will be published
2	Code for the calculation of hydrogen adsorption in porous nanostructured materials	TH	The code is publicly available at https://www.jacobs-university.de/ses/theine/research
3	Improved Density Functional based tight-binding method with computer code	TH	Two software versions of the code are available. The first one is public (https://www.jacobs-university.de/ses/theine/research), the second commercially exploited through QUASINANO (www.scm.com)
4	DFT code and implementation procedures	TM	The code is available to academic community within the deMon package (www.demon-software.com)

5	EMBED computational package	NR	The code is available from the authors
6	Novel dopants for material hybrids and MOFs to improve hydrogen storage	PKC (Indian partner)	none
7	New catalysts for dehydrogenation of boron nitrides	NR	publication
8	Catalysts to release hydrogen from hydrocarbons	NR	publication
9	Database of hydrogen storage capabilities for nanoporous materials	SK (Indian Partner)	Compilation in progress, will become publicly available
10	Database of diffusion constants of gases in nanoporous material	KV (Indian Partner)	Available on project website
11	Database of proton diffusion rates in ceramic materials	CA	Available on project website
12	Database of proton diffusion rates in high temperature membranes	CA	Available on project website
13	Nanoporous materials for simultaneous chemisorption and physisorption	TH	publication
14	Design of new protonic ceramics and polymers	CA	publication
15	Training materials	All	In individual use

Scientific exploitation: The results have been used for publication, as discussed in the dissemination section.

Exploitation of the networking activities and method development: A joint FP7-MC-IRSES project was successfully applied and three partners continue collaborating within the network TEMM1P.

Please provide the public website address (if applicable), as well as relevant contact details.
The project website will remain available under https://www.jacobs-university.de/ses/theine/projects/HYPOMAP

References

[1] S. Patchkovskii, T. Heine, *Physical Review E* **2009**, *80*.
[2] B. Lukose, M. Wahiduzzaman, A. Kuc, T. Heine, *Submitted to Journal of Physical Chemistry C* **2012**.
[3] M. Rapacioli, F. Spiegelman, D. Talbi, T. Mineva, A. Goursot, T. Heine, G. Seifert, *Journal of Chemical Physics* **2009**, *130*.
[4] V. Tognetti, C. Adamo, *Journal of Physical Chemistry A* **2009**, *113*, 14415-14419.
[5] aT. A. Maark, S. Pal, *International Journal of Hydrogen Energy* **2010**, *35*, 12846-12857; bM. Dixit, T. A. Maark, S. Pal, *International Journal of Hydrogen Energy* **2011**, *36*, 10816-10827.
[6] M. Prakash, M. Elango, V. Subramanian, *International Journal of Hydrogen Energy* **2011**, *36*, 3922-3931.
[7] aR. M. Kumar, V. Subramanian, *International Journal of Hydrogen Energy* **2011**, *36*, 10737-10747; bK. Gopalsamy, M. Prakash, R. M. Kumar, V. Subramanian, *International Journal of Hydrogen Energy* **2012**, *37*, 9730-9741.
[8] K. Srinivasu, S. K. Ghosh, *Journal of Physical Chemistry C* **2011**, *115*, 16984-16991.

[9] K. Srinivasu, K. R. S. Chandrakumar, S. K. Ghosh, *Journal of Physical Chemistry A* **2010**, *114*, 12244-12250.
[10] K. Srinivasu, S. K. Ghosh, *prepared for publication* **2012**.
[11] S. Chowdhury, F. Himo, N. Russo, E. Sicilia, *Journal of the American Chemical Society* **2010**, *132*, 4178-4190.
[12] M. d. C. Michelini, J. Marcalo, N. Russo, J. K. Gibson, *Inorganic Chemistry* **2010**, *49*, 3836-3850.
[13] A. Chakraborty, S. Duley, S. Giri, P. K. Chattaraj, *An Understanding of the Origin of Chemical Reactivity from a Conceptual DFT approach*, John Wiley, **2010**.
[14] P. K. Chattaraj, S. Duley, *Journal of Chemical and Engineering Data* **2010**, *55*, 1882-1886.
[15] aS. Giri, A. Chakraborty, P. K. Chattaraj, *Journal of Molecular Modeling* **2011**, *17*, 777-784; bS. Bandaru, A. Chakraborty, S. Giri, P. K. Chattaraj, *International Journal of Quantum Chemistry* **2012**, *112*, 695-702; cS. Pan, G. Merino, P. K. Chattaraj, *Physical Chemistry Chemical Physics* **2012**, *14*, 10345-10350.
[16] S. Pan, S. Giri, P. K. Chattaraj, *Journal of Computational Chemistry* **2012**, *33*, 425-434.
[17] K. Srinivasu, S. K. Ghosh, R. Das, S. Giri, P. K. Chattaraj, *Rsc Advances* **2012**, *2*, 2914-2922.
[18] A. Chakraborty, S. Giri, P. K. Chattaraj, *Structural Chemistry* **2011**, *22*, 823-837.
[19] A. Chakraborty, S. Duley, P. K. Chattaraj, *Indian Journal of Chemistry Section a-Inorganic Bio-Inorganic Physical Theoretical & Analytical Chemistry* **2012**, *51*, 226-244.
[20] P. K. Chattaraj, R. Das, S. Duley, S. Giri, *Aromaticity and conceptual density functional theory*, RSC Publishing, **2011**.
[21] S. Duley, S. Giri, N. Sathyamurthy, R. Islas, G. Merino, P. K. Chattaraj, *Chemical Physics Letters* **2011**, *506*, 315-320.
[22] S. Giri, S. Bandaru, A. Chakraborty, P. K. Chattaraj, *Physical Chemistry Chemical Physics* **2011**, *13*, 20602-20614.
[23] K. Srinivasu, K. R. S. Chandrakumar, S. K. Ghosh, *Chemphyschem* **2009**, *10*, 427-435.
[24] N. K. Jena, K. Srinivasu, S. K. Ghosh, *Journal of Chemical Sciences* **2012**, *124*, 255-260.
[25] K. Srinivasu, S. K. Ghosh, *International Journal of Hydrogen Energy* **2011**, *36*, 15681-15688.
[26] K. Srinivasu, S. K. Ghosh, *Journal of Physical Chemistry C* **2011**, *115*, 1450-1456.
[27] K. Srinivasu, S. K. Ghosh, *Journal of Physical Chemistry C* **2012**, *116*, 5951-5956.
[28] P. K. Chattaraj, S. Bandaru, S. Mondal, *Journal of Physical Chemistry A* **2011**, *115*, 187-193.
[29] A. Pal, K. Vanka, *Chemical Communications* **2011**, *47*, 11417-11419.
[30] K. Ghatak, K. Vanka, *Computational and Theoretical Chemistry* **2012**, *992*, 18-29.
[31] V. Butera, N. Russo, E. Sicilia, *Chemistry-a European Journal* **2011**, *17*, 14586-14592.
[32] K. Ghatak, K. Vanka, *Submitted to Journal of Molecular Structure* **2012**.
[33] M. P. Ljungberg, J. J. Mortensen, L. G. M. Pettersson, *Journal of Electron Spectroscopy and Related Phenomena* **2011**, *184*, 427-439.
[34] P. Jha, L. Petterson, *Manuscript in preparation* **2012**.
[35] L. Chen, A. C. Cooper, G. P. Pez, H. Cheng, *Journal of Physical Chemistry C* **2007**, *111*, 18995-19000.
[36] R. Bhowmick, S. Rajasekaran, D. Friebel, C. Beasley, L. Jiao, H. Ogasawara, H. Dai, B. Clemens, A. Nilsson, *Journal of the American Chemical Society* **2011**, *133*, 5580-5586.
[37] K. Srinivasu, S. K. Ghosh, *Prepared for publication* **2012**.
[38] Y. Lin, F. Ding, B. I. Yakobson, *Physical Review B* **2008**, *78*.
[39] aK. Andersson, A. Nikitin, L. G. M. Pettersson, A. Nilsson, H. Ogasawara, *Physical Review Letters* **2004**, *93*; bA. Nikitin, X. Li, Z. Zhang, H. Ogasawara, H. Dai, A. Nilsson, *Nano Letters* **2008**, *8*, 162-167; cA. Nikitin, L.-A. Naeslund, Z. Zhang, A. Nilsson, *Surface Science* **2008**, *602*, 2575-2580; dA. Nikitin, Z. Zhang, A. Nilsson, *Nano Letters* **2009**, *9*, 1301-1306.
[40] P. Strasser, S. Koh, T. Anniyev, J. Greeley, K. More, C. Yu, Z. Liu, S. Kaya, D. Nordlund, H. Ogasawara, M. F. Toney, A. Nilsson, *Nature Chemistry* **2010**, *2*, 454-460.
[41] T. Anniyev, H. Ogasawara, M. P. Ljungberg, K. T. Wikfeldt, J. B. MacNaughton, L.-A. Naslund, U. Bergmann, S. Koh, P. Strasser, L. G. M. Pettersson, A. Nilsson, *Physical Chemistry Chemical Physics* **2010**, *12*, 5694-5700.

[42] aD. Friebel, D. J. Miller, C. P. O'Grady, T. Anniyev, J. Bargar, U. Bergmann, H. Ogasawara, K. T. Wikfeldt, L. G. M. Pettersson, A. Nilsson, *Physical Chemistry Chemical Physics* **2011**, *13*, 262-266; bD. J. Miller, H. Oberg, S. Kaya, H. S. Casalongue, D. Friebel, T. Anniyev, H. Ogasawara, H. Bluhm, L. G. M. Pettersson, A. Nilsson, *Physical Review Letters* **2011**, *107*; cD. J. Miller, H. Oberg, L. A. Naslund, T. Anniyev, H. Ogasawara, L. G. M. Pettersson, A. Nilsson, *Journal of Chemical Physics* **2010**, *133*.
[43] T. Zambelli, J. V. Barth, J. Wintterlin, G. Ertl, *Nature* **1997**, *390*, 495-497.
[44] T. Anniyev, H. Oberg, S. Kaya, H. Ogasawara, D. Nordlund, D. Friebel, D. J. Miller, U. Bergmann, L. G. M. Petterson, A. Nilsson, *Submitted to Journal of Physical Chemistry C* **2012**.
[45] R. Das, P. K. Chattaraj, *Journal of Physical Chemistry A* **2012**, *116*, 3259-3266.
[46] A. Martinez-Mesa, S. N. Yurchenko, S. Patchkovskii, T. Heine, G. Seifert, *Journal of Chemical Physics* **2011**, *135*.
[47] A. Kuc, T. Heine, T. Mineva, *Submitted to Structure Chemistry* **2012**.
[48] K. Srinivasu, S. K. Ghosh, *Prepared for publication* **2012**.
[49] G. F. Mangiatordi, J. Hermet, C. Adamo, *Journal of Physical Chemistry A* **2011**, *115*, 2627-2634.
[50] G. F. Mangiatordi, V. Butera, N. Russo, C. Adamo, *Prepared for publication* **2012**.
[51] M. Prakash, V. Subramanian, *Physical Chemistry Chemical Physics* **2011**, *13*, 21479-21486.
[52] S. Giri, A. Chakraborty, P. K. Chattaraj, *Nano Reviews* **2011**, *2*, 5767.